Sedimentary Geology 460 (2024) 106561

Contents lists available at ScienceDirect

Sedimentary Geology

journal homepage: www.elsevier.com/locate/sedgeo

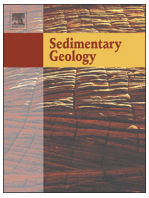

Increased sediment connectivity between deltas and deep-water fans in closed lake basins: A case study from Bozhong Sag, Bohai Bay Basin, China

Puyu Liu [a,b], Chenglin Gong [a,b,*], James H. Gearon [c], Dayong Guan [d], Qiming Wang [d], Kun Qi [a,b], Dongwei Li [a,b]

[a] National Key Laboratory of Petroleum Resources and Engineering, China University of Petroleum (Beijing), Beijing 102249, China
[b] College of Geosciences, China University of Petroleum (Beijing), Beijing 102249, China
[c] Department of Earth and Atmospheric Sciences, Indiana University, 1001 East 10th Street, Bloomington, IN 47408, USA
[d] Bohai Oilfield Research Institute, Tianjin Branch of China National Offshore Oil Corporation Ltd., Tianjin 300452, China

ARTICLE INFO

Article history:
Received 9 September 2023
Received in revised form 3 December 2023
Accepted 9 December 2023
Available online 16 December 2023

Editor: Dr. Catherine Chagué

Keywords:
Deltaic clinothems
Sequence stratigraphy
Sub-lacustrine fans
Sediment connectivity
Bohai Bay Basin

ABSTRACT

The connection between deltaic clinothem growth and the formation of down-dip deep-water systems on continental margins has been extensively discussed as a crucial component of sequence stratigraphic theory. However, in lacustrine settings, the growth of deltaic clinothems and outlying deep-water fans remains comparatively poorly understood. In the southwestern Bozhong Sag, Bohai Bay Basin, China, both lacustrine deltas and outlying sub-lacustrine fans were developed during the Oligocene, providing an opportunity to investigate the connection between lacustrine deltaic clinothem growth and the formation of outlying sub-lacustrine fans in deep-lacustrine systems. We employ 3D seismic data, well data, core data, and sandstone grainsize data to analyze the stacking patterns and internal architectures of these two sedimentary systems in the lower and upper successions of our study interval, SQEd_2^L. In addition, elemental geochemical parameters were utilized to reveal the paleoclimatic signature of the different stratigraphic successions. Our results suggest that there are two main types of deltaic clinothem stacking patterns in the lower and upper successions of SQEd_2^L, respectively: (1) in the lower succession, progradational to aggradational stacking patterns have a flat to steeply rising rollover trajectory, and (2) in the upper succession, aggradational to progradational and degradational stacking patterns have a slightly rising to flat and slightly falling trajectory. Meanwhile, the sub-lacustrine fans with straight channels and thick lobe complexes are coupled with progradational and aggradational (PA) deltaic clinothems in the lower succession. In the upper succession, small-scale sub-lacustrine fans with sinuous channels and thin lobe complexes are coupled with aggradational to progradational and degradational (APD) deltaic clinothems. The sediment connectivity between lacustrine deltas and sub-lacustrine fans stands in stark contrast to their counterparts in marine basins (such as marine APD clinothems coupled with large-scale deep-water fans, while marine PA clinothems rarely produce deep-water fans). In addition, two contrasting paleoclimatic stages have been identified in SQEd_2^L, namely the earlier humid stage in the lower succession and the later semiarid climatic stage in the upper succession. A comprehensive analysis of the differences between lacustrine and marine basins indicates that climatic variations play a pivotal role in deep-lacustrine deposition. Consequently, a climate-cycle-driven, sediment-supply-dominated sedimentary model of delta-to-fan sediment connectivity is proposed that incorporates the efficiency of terrigenous sediment dispersal into deep-lacustrine floors and the architecture of sub-lacustrine fans. The findings of this study further refine the implementation of the sequence stratigraphy paradigm and enhance the understanding of delta-to-fan sediment connectivity in deep-lacustrine depositional systems.

1. Introduction

Deltas and submarine fans are the two primary sedimentary systems on the continental margins. As such, they attract considerable attention from sedimentologists because of their implications for the dispersal of terrigenous sediments to deep-water sites (Covault et al., 2007; Henriksen et al., 2011a; Dixon et al., 2012; Gong et al., 2015b, 2021).

As deltas advance across the shelf they can deliver sediment to deep-water sites, forming submarine fans and over time build sedimentary prisms (e.g., Henriksen et al., 2011b; Bahka et al., 2017; Paumard et al., 2019; Zhang et al., 2019). Within these prisms exist deltaic clinoforms, discrete phases of deltaic aggradation and accretion

* Corresponding author at: College of Geosciences, China University of Petroleum (Beijing), 18 Fuxue Road, Changping, Beijing 102249, China.
E-mail address: chenglingong@cup.edu.cn (C. Gong).

https://doi.org/10.1016/j.sedgeo.2023.106561
0037-0738/

bounded by chronostratigraphic surfaces (Johannessen and Steel, 2005; Houseknecht et al., 2009; Fongngern et al., 2016). The equivalent lithological units bounded by these clinoforms and located at the shelf margin or slope break are deltaic clinothems (Sztanó et al., 2013; Pellegrini et al., 2020; J. Liu et al., 2020; Qi et al., 2023). In marine settings, such as shelf margins of the Yinggehai and Qiongdongnan basins, stacking patterns of the deltaic clinothems are closely related to coeval deep-water fans, which can indicate sediment transport and dispersal from the terrigenous to deep-water sites (Gong et al., 2015b, 2019). The relationship between marine deltaic clinothems and deep-water fans has been increasingly studied in recent years (e.g., Fisher et al., 2021; Gong et al., 2021; Qi et al., 2023).

In the source-to-sink system, terrigenous sediments are transported via rivers and deposited by deltas on the shelf. Some deltas are capable of dispersing sediments further into deep-water, forming submarine fans (Dixon et al., 2012; Sømme and Jackson, 2013; Chen et al., 2021). In these connected settings, deltas and fans act as secondary "sources" and "sinks" in the subaqueous portion of the source-to-sink system, respectively (Gong et al., 2021). Previous work has demonstrated that the growth of deltaic clinothems is coupled to the growth of submarine fans in marine settings (e.g., Gong et al., 2021). In contrast to marine systems, the coupling relationship between lacustrine deltas and sub-lacustrine fans is comparatively unconstrained.

Previous work has emphasized that lakes are not just small oceans and that classical sequence stratigraphic theory cannot be mechanically applied to the study of lacustrine depositional systems (e.g., Carroll and Bohacs, 1999; Gong et al., 2019; Gearon et al., 2022). The significant differences between lakes and oceans are: (1) Lake levels vary more rapidly than sea levels (i.e., 300 m in 15 ky is not uncommon in Lake Turkana, Kenya; Johnson et al., 1987; Haq et al., 1987; Kroonenberg et al., 1997; Huybers et al., 2016). (2) Lake level and river discharge are highly coupled compared to marine settings; lake level falls when river discharge falls, and vice versa (i.e., the variability of the Chari River discharge can predict the height of lake level in the Lake Chad basin; Coe and Birkeet, 2004; Lyons et al., 2011; Gong et al., 2019). (3) Changes in salinity play an influential role in the partitioning of river-borne sediments in closed lake basins through the occurrence of hyperpycnal flows (e.g., Bohacs et al., 2000; Zavala et al., 2006; Lamb et al., 2010). (4) Regional climatic shifts may affect riverine discharge variability and, therefore, the transmission of sediment and water into the closed lake basin (e.g., Gearon et al., 2022).

Here, we examined Oligocene-aged lacustrine deltas and sub-lacustrine fans in southwestern Bozhong Sag, Bohai Bay Basin, to investigate whether lacustrine deltas and deep-water fans demonstrate marine-style sediment connectivity. Using integrated 3D seismic data, well data, core data, and grainsize data provided in this study and geochemical data acquired from previous studies, we quantify stacking patterns of lacustrine deltaic clinothems and the sedimentary characteristics of sub-lacustrine fans. We additionally analyze the specific mechanisms of this relationship within the paradigm of climate-driven, supply-dominated sediment connectivity in lacustrine depositional systems.

2. Geological background

The Bohai Bay Basin, located in eastern China, is a petroliferous, Cenozoic-aged continental lacustrine rift basin that covers ~200,000 km^2 and comprises seven sub-basins: Bozhong, Liaohe, Liaodong Bay, Huanghua, Jizhong, Jiyang, and Linqing (Feng et al., 2016; Ji et al., 2022) (Fig. 1A). In the central part of the Bozhong sub-basin, near the offshore area (i.e., the Bohai Sea), lies the Bozhong Sag, which covers a total area of 3000 km^2 (Fig. 1A). The Sag is a closed lake basin bounded by the Shaleitian Uplift in the west, the Shijiutuo Uplift in the north, the Bonan Low Uplift in the south, and the Bodong Low Uplift in the east (Zhu et al., 2014; Li et al., 2019) (Fig. 1A, B). Our study focuses on the southwestern segment of the Bozhong Sag, which is flanked by a slope break to the south and a subsidence center to the north (Fig. 1C).

The Bozhong Sag underwent two major stages of tectonic evolution, namely the syn-rift stage (65.0 Ma–24.6 Ma) and the post-rift stage (24.6 Ma–present) (Wang et al., 2017; Yu et al., 2020). Generally, the syn-rift stage of the Bozhong Sag can be divided into four distinct episodes: the initial rifting stage (episode I), the stretching rifting stage (episode II), the thermal subsidence stage (episode III), and the strike-slip rifting stage (episode IV) (Zhu et al., 2021) (Fig. 2). These episodes correspond to the deposition of the Kongdian Formation and the lower part of the Shahejie Formation (65.0 Ma–42.0 Ma), the middle part of the Shahejie Formation (42.0 Ma–38.0 Ma), the upper part of the Shahejie Formation (38.0 Ma–32.8 Ma), and the Dongying Formation (32.8 Ma–24.6 Ma), respectively (Feng et al., 2016; Zhu et al., 2021) (Fig. 2). More specifically, the Oligocene Dongying Formation is further divided into four members from base to top: the third member (Ed_3), the lower part of the second member (Ed_2^L), the upper part of the second member (Ed_2^U), and the first member (Ed_1). These members correspond to the third sequence of SQEd_3, SQEd_2^L, SQEd_2^U, and SQEd_1 (Xu et al., 2020; Xia et al., 2022) (Fig. 2). Previous studies have summarized the principal depositional systems of the Dongying Formation, including: (1) fluvial deltaic deposits that developed during the later depositional stage of the Dongying Formation; (2) proximal fan deltas deposited near the foot of the hanging wall of the bounding fault; (3) braided deltas deposited on the slope; and (4) sub-lacustrine fans deposited in front of the delta front or in the basin center (Xu et al., 2020; Li et al., 2021) (Figs. 1B, 2).

Our primary study interval, SQEd_2^L, was formed during the strike-slip rift stage of a relatively stable tectonic period. The present stratal thickness of SQEd_2^L is more than 600 m, and the main facies of lacustrine deltas, sub-lacustrine fans and deep-lacustrine mudstones in the SQEd_2^L form the deep-lacustrine depositional systems (Xu et al., 2020; Li et al., 2021; Ji et al., 2022) (Figs. 1B, 2). Moreover, the presence of *Ostracoda* fossil assemblages in SQEd_2^L indicates a deep-water, humid-to-semiarid depositional environment (Feng et al., 2016), which was also reported by Yang et al. (2021) using palynological and geochemical evidence.

3. Database and methodology

3.1. 3D seismic data, well data core data, and geochemical data

The primary datasets utilized in this study include 800 km^2 of three-dimensional (3D) seismic, wireline logs, cores, grain-size data, and geochemical data, all of which were acquired from the Bozhong Sag (Fig. 1C) and provided by the Tianjin Branch of China National Offshore Oil Corporation (CNOOC). The 3D seismic data were acquired with a 4-millisecond sampling interval and a bin size spacing of 25 m (in-line) by 12.5 m (cross-line). These data were processed using a post-stack hybrid migration algorithm, and they have a dominant frequency of 15.83 m–31.67 m ($\lambda/4$) and a detection limit of 2.53 m–5.07 m ($\lambda/25$). The SEG negative standard polarity was employed to display the data, where a positive reflection coefficient corresponds to an increase in acoustic impedance and reflects a negative reflection event. They are shown using a blue–white–red color bar, with the low-impedance top of the reservoir being a peak (blue). The 3D seismic data were tied to 10 wells (Fig. 1C), each of which has lithologies and high-quality well-logging curves including gamma ray (GR), acoustic (AC), spontaneous potential (SP), and density (DEN). The sonic and density logs, check shots, and formation markers obtained from 10 wells (Fig. 1C) were carefully processed. Well-log data were also utilized to constrain seismic-well ties and ages to determine the age and geological significance of the major seismic reflections.

This investigation is also predicated upon the utilization of 49 assemblages of sandstone core data and grainsize data (comprising 3 sections of core samples from Well-B61, spanning the depth interval of 4052.50 m–4072.00 m; and 46 sections of core samples from Well-A23, spanning the depth interval of 4166.00 m–4464.00 m) (Fig. 1C) provided by the Bohai Petroleum Research Institute of CNOOC, serving as

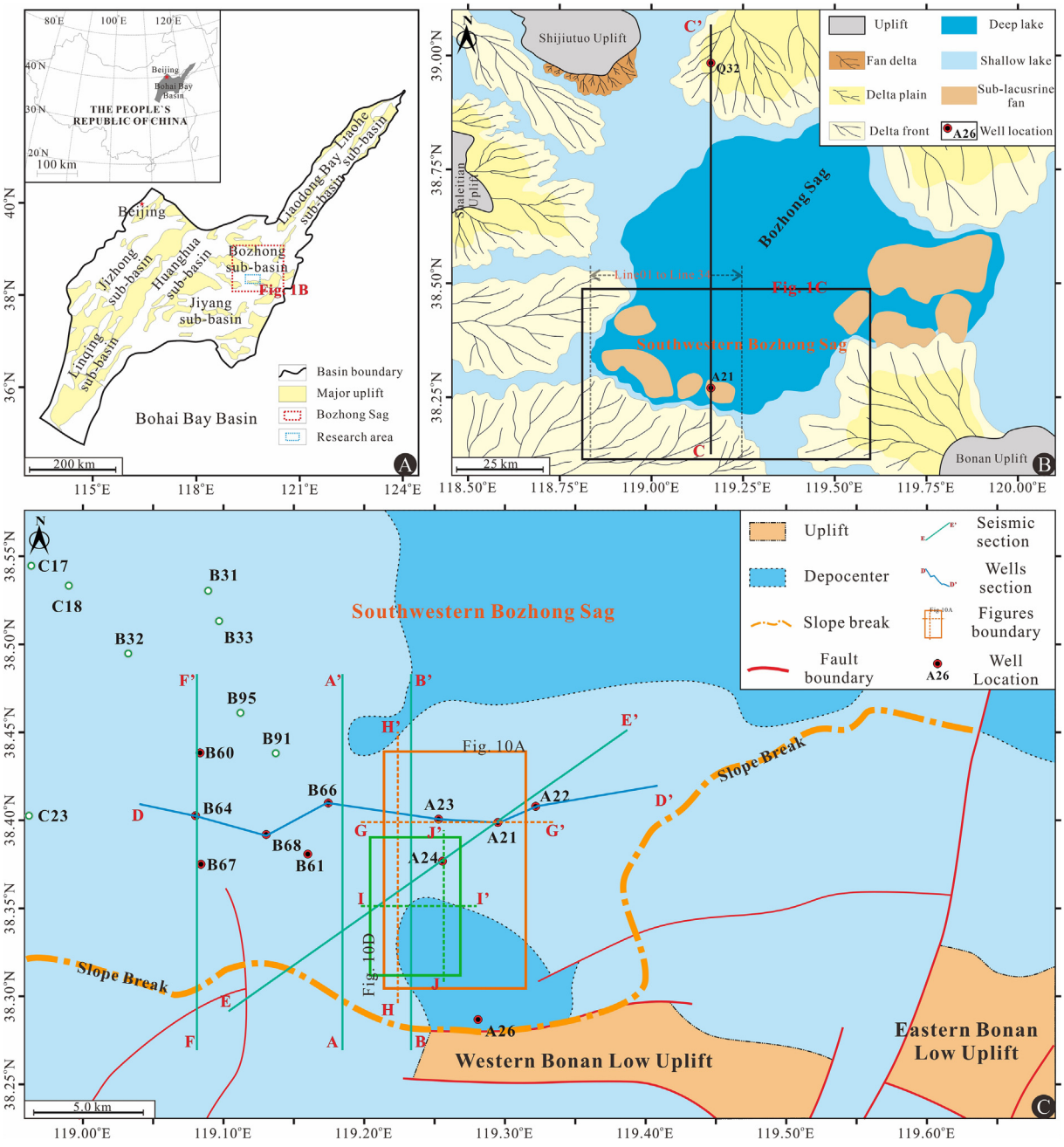

Fig. 1. Geological setting of the study area. (A) Location of Bohai Bay Basin and the study area (blue dotted box). (B) Depositional facies of the SQEd_2^L in the southwestern Bozhong Sag, Bohai Bay Basin (adapted from Xu et al., 2020; Li et al., 2021). (C) Map showing the well location, seismic section, and structural division of the Oligocene southwestern Bozhong Sag.

compelling substantiation for the interpretation of sedimentary types. Furthermore, the grainsize data of the core samples was determined using the Laser Diffraction Particle Size Analyzers-Malvern Panalytical (MS2000/MAL1099796) at the Bohai Petroleum Experimental Center of CNOOC. Ultimately, the amalgamation of two sets of sandstone core samples, grainsize distribution frequency, and grainsize accumulation frequency, in conjunction with the typical root-mean-square (RMS) amplitude stratal slices and well logging data, was employed to expound upon the sedimentary types prevalent within the Oligocene southwestern Bozhong Sag.

The geochemical data primarily pertain to the content of major and trace elements, as well as their relative ratios, in the 135 sets of dark mudstone samples acquired from eight wells (B31, B32, B33, B91, B95, C17, C18, and C19) (Fig. 1C) in the Dongying Formation of southwestern Bozhong Sag. All of the dark mudstone samples were tested and analyzed by X-Ray Fluorescence Spectrometers (ZSX Primus II) and an Inductively Coupled Plasma Mass Spectrometer (PE 350X). Consequently, the contents of major elements (such as *CaO*, *MgO*, Na_2O, Al_2O_3, Fe_2O_3, and other 12 types of oxides) and trace elements (such as *Cu*, *Th*, *U*, *Sr*, *Co*, and other 30 types of trace elements) were obtained for each of the dark mudstone samples, respectively. These two types of experiments were conducted at the Bohai Petroleum Experimental Center of CNOOC, and the original data for the experiments were sourced from Yang et al. (2021), which serves as a crucial tool for reconstructing the paleoclimate fluctuations during the sedimentation of the southwestern Bozhong Sag.

3.2. Seismic interpretation and quantification of deltaic clinothems

Seismic interpretation was made using the GeoFrame Seiswork software, and a workflow was designed for interpreting the seismic

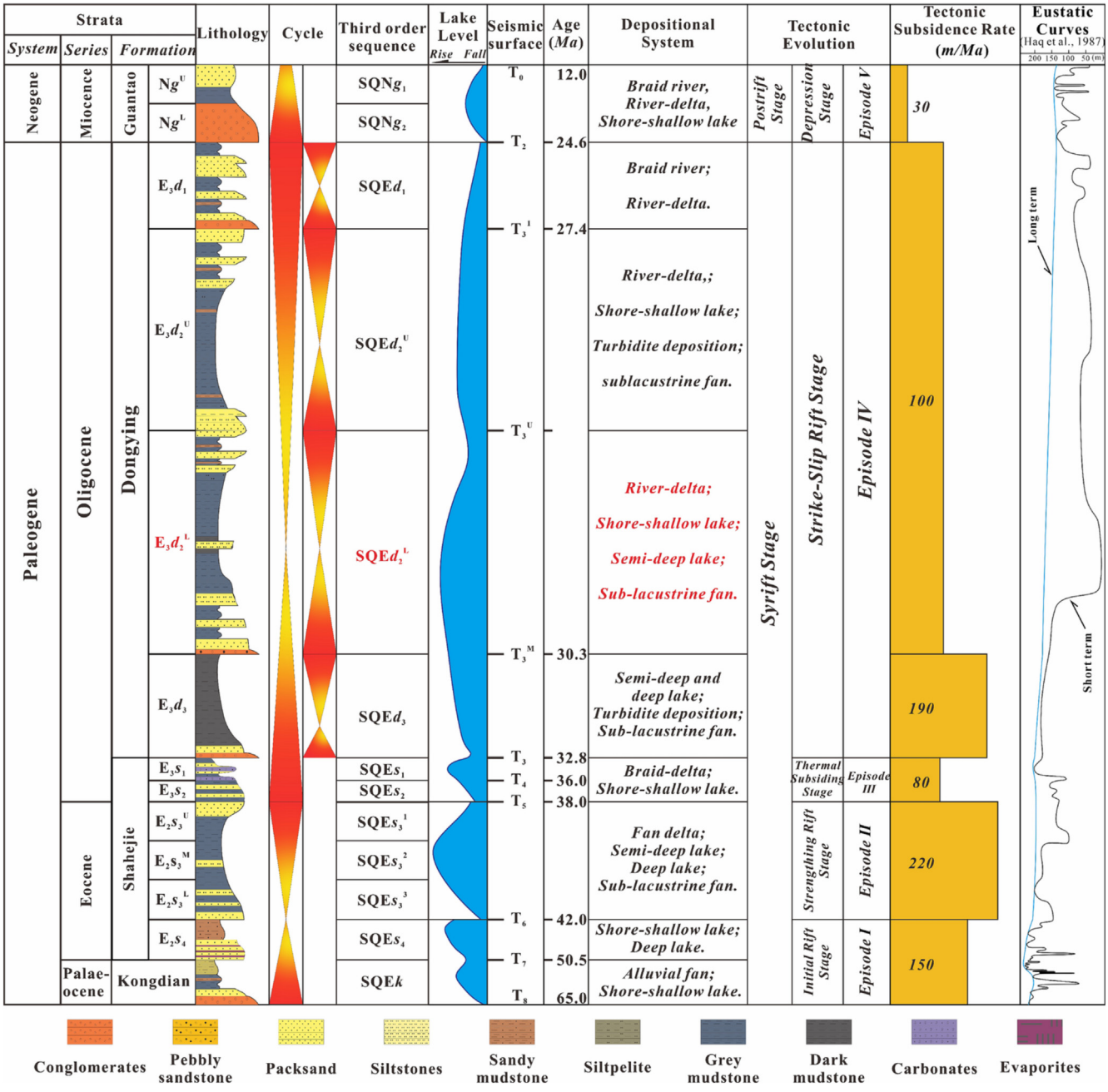

Fig. 2. Generalized Paleogene lithostratigraphy, sequence stratigraphy, depositional systems, and tectonic evolution of Bozhong Sag, Bohai Bay Basin, China (adapted from Feng et al., 2016; Zhu et al., 2021; Ji et al., 2022). The study interval in this study is $SQEd_2^L$, which corresponds to the lower part of the second member of the Dongying Formation.

stratigraphy of the southwestern Bozhong Sag. This workflow is based on the use of 3D volume seismic interpretation tools in combination with a standard seismic stratigraphic approach in which reflection terminations are used for identifying seismic unconformities (sensu Mitchum and Wagoner, 1991). Within the Oligocene Dongying Formation of the study area, this workflow helped us to identify major regional seismic unconformities and their corresponding conformity interfaces as sequence boundaries. Meanwhile, utilizing the technique of flattening seismic volumes to the basin-wide unconformity of T_3^1 (dated approximately at 27.4 Ma) may be beneficial for seismic interpretation and quantification of deltaic clinothems within the Oligocene Dongying Formation (Yu et al., 2021; Zhao et al., 2021).

In this study, three crucial principles were invoked for characterizing lacustrine deltaic clinothems and quantifying sediment partitioning to lacustrine basin floors. First, stratal terminations, including toplap and downlap terminations, were used as indicators of sediment partitioning in lacustrine basins. For example, erosional terminations of toplap are symptomatic of topset erosion and the consequent delivery of sediments to deep-water sites, whereas aggradational topsets are indicative of topset storage of terrestrial sediments (e.g., Paumard et al., 2018; Yu et al., 2021). Second, the relative amount of sediment partitioned into the topset compartment of a clinothem set can be roughly estimated from the topset thickness (T_t) of individual clinothem sets (Gong et al., 2019; E. Liu et al., 2020; J. Liu et al., 2020; Yu et al., 2021). Third, the relative amount of sediment dispersed into deep-lake areas can be roughly estimated from the bottomset thickness (T_b) of individual clinothem sets (Fig. 3B, D) (Gong et al., 2015a, 2019; Yu et al., 2021; Zhao et al., 2021).

The growth patterns and architectural styles of the recorded lacustrine deltaic clinothem sets were quantified by measuring the distance between the forward progradational rollover point and the prior rollover point (d_x), the vertical aggradational rollover point (d_y), and the

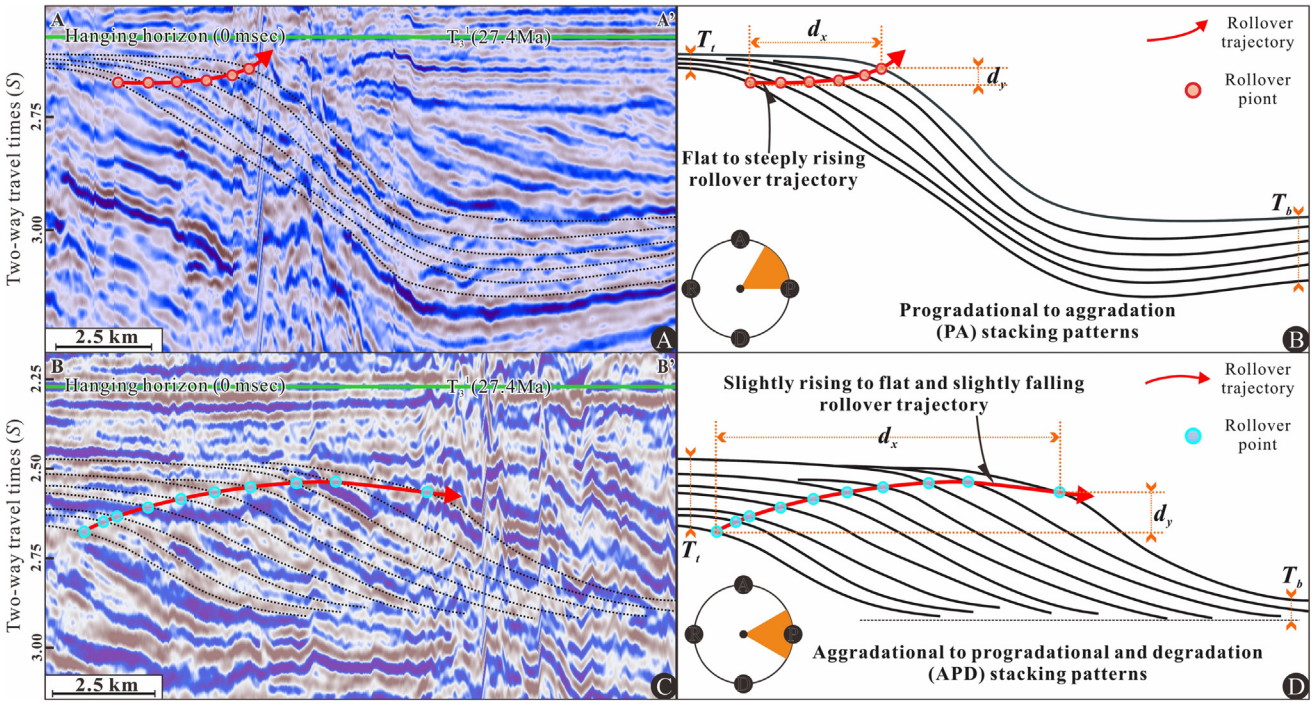

Fig. 3. Dip-view seismic profiles and line drawings showing cross-sectional expressions (A–A′ and B–B′, see location in Fig. 1C), measurement parameters, and architectural styles of two stratal stacking patterns of lacustrine deltaic clinothems in the lower succession (A, B) and upper succession (C, D). A = aggradation; P = progradation; D = degradation; R = retrogradation. The shown seismic lines were flattened by T_3^l unconformity dated at 27.4 Ma, in order to restore paleohorizons and original patterns of the documented clinothem sets and their associated topset-to-foreset rollover trajectories.

trajectory angle (T_r), which was calculated from the following formula (Fig. 3B, D) (e.g., Gong et al., 2015a; Yu et al., 2021; Zhao et al., 2021):

$$T_r = \tan^{-1}(d_x/d_y)$$

To quantify the characteristics of the documented lacustrine deltaic clinothems and their relationship to sediment dispersal to the lacustrine basin floor, we used the parameters of topset-to-foreset rollover trajectories (d_x, d_y, and T_r) and lacustrine deltaic clinothem architectures (T_t, T_b, and T_t/T_b). Additionally, we also converted the measured parameters of d_x, d_y, T_r, T_t, and T_b from time to depth using an average velocity of 3800 m/s. To effectively remove post-Oligocene deformation and differential compaction-related subsidence, and to accurately measure the five parameters of the deltaic clinothems, it is necessary to preprocess the seismic data to restore the intrinsic characteristics of the lacustrine deltaic clinothems. We flattened the seismic cube using the sequence boundary above the study interval (T_3^l, dated at 27.4 Ma) as the hanging horizon, and the influences of stratigraphic deformation and differential compaction after the deposition of the study interval can be excluded (e.g., Yu et al., 2021; Zhao et al., 2021) (Fig. 3A, C). As a result, we selected a total of 34 representative seismic profiles to measure the above 5 parameters, providing us with 34 sets of data on the stacking patterns of lacustrine deltaic clinothems.

4. Stratigraphic framework and depositional styles of SQEd_2^L

4.1. Stratigraphic framework of SQEd_2^L

In the studied SQEd_2^L (i.e., the lower part of the 2nd member of the Dongying Formation), three distinct unconformities are identified from the seismic sections and well profiles (Figs. 4, 5). They are T_3^u, T_3^m, and MFS, respectively, where T_3^u and T_3^m represent the upper and lower sequence boundaries of SQEd_2^L, and MFS represents the Maximum Flooding Surface (the following Maximum Flooding Surface is indicated by MFS) within the studied SQEd_2^L (Figs. 4, 5).

As the upper sequence boundary of SQEd_2^L, the T_3^u is well represented by an erosional unconformity. This unconformity is distinguishable by continuous and high-amplitude reflection terminations, with regional toplap contacts visible in the seismic sections (Fig. 4). In the well-log profiles, T_3^u generally exhibits an abrupt change along the unconformity, and cylindrical gamma-ray (GR) curves appear above the unconformity in wells B64, B68, and A21 (Fig. 5). In the lower sequence boundary of SQEd_2^L, T_3^m is displayed as an extensive erosional unconformity, which is visible in the seismic sections (Fig. 4). Along the unconformity, relatively strong amplitudes and continuity exist, and onlap contacts against the slope break can be observed. In the well-log profiles, T_3^m is commonly associated with abrupt changes, such as box-shaped and finger-shaped GR curves above T_3^m (Fig. 5).

The MFS within SQEd_2^L exhibits moderate amplitudes and continuity. This surface can be identified as the downlap contact interface of SQEd_2^L in the seismic profiles (Fig. 4). The corresponding well-log data commonly display the development of mudstones and high GR values, and the grain size of the lithology gradually decreases toward the maximum flooding surface (Fig. 5). Because of the presence of these three unconformities, the studied SQEd_2^L can be divided into two successions, lower and upper (Figs. 4, 5).

4.2. Depositional styles of SQEd_2^L

Through an integrated analysis of grain size, lithofacies association, log facies, and seismic facies, three distinct depositional styles have been identified in SQEd_2^L (Table 1). The first depositional style has interbedded mudstone and thin-layered sandstone or siltstone, which generally correspond to an inversed cycle of the GR value in the well profile (Table 1). In seismic data, the first depositional style mainly consists of large-scale progradation-dominated seismic facies, which have moderate amplitude and continuous reflectors with oblique or sigmoidal geometries (Table 1). In the typical root-mean-square (RMS) amplitude stratal slices, the first depositional style tends to advance toward the depocenter of the Bozhong Sag (Table 1). According to these descriptions, the first

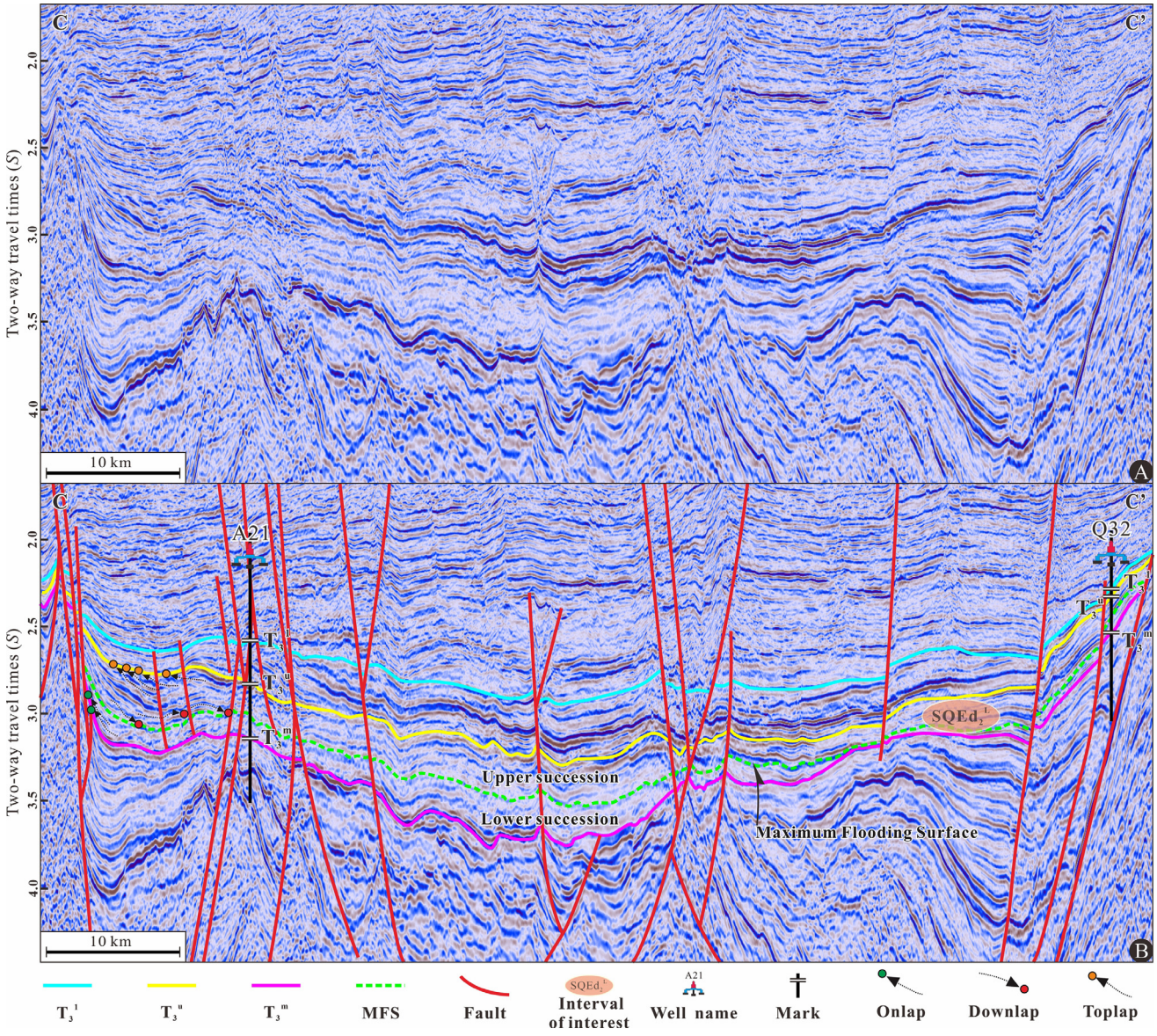

Fig. 4. Uninterpreted (A) and interpreted (B) regional 2D seismic profiles (C–C′, see location, Fig. 1B) showing the main seismic unconformities and their downslope correlative conformities (T_3^u, T_3^m, and MFS), which bound the lower and upper successions. The lower succession shows an onlap phenomenon, and the upper succession shows toplap and downlap phenomena in the seismic sections.

depositional style has been interpreted as lacustrine deltaic deposits (e.g., Liu et al., 2014; Fongngern et al., 2018; E. Liu et al., 2020;Olariu et al., 2022; Würtzen et al., 2022).

The second depositional style has a higher sand content, and the frequency distribution of clastic particles in the sandstone displays a bimodal pattern (Table 1). Additionally, the grainsize frequency is characterized by a double peak, and the cumulative-frequency curve of the sandstone grain size exhibits a two-segmented shape, with the saltating population being the dominant component of the sediment gravity flow deposition (Wu et al., 2023) (Table 1). Corresponding to the log facies of the GR value, the second depositional style is typified by box-shaped and finger-shaped structures (Table 1). In seismic sections, this second depositional style shows two distinct seismic facies: small-scale uniform and continuous seismic facies and large-scale irregular seismic facies (Table 1). In the typical root-mean-square (RMS) amplitude stratal slices, these seismic facies are expressed as fan-like shapes. Therefore, the second depositional style has been interpreted as sub-lacustrine channel–lobe systems (e.g., Liu et al., 2014; E. Liu et al., 2020; J. Liu et al., 2020; Wu et al., 2022; Yang et al., 2023b).

The third depositional style is ubiquitous within the SQEd_2^L of the Oligocene southwestern Bozhong Sag. This style has a lower sand content corresponding to a zigzag log pattern, and a higher GR value (Table 1). In seismic sections, this style is represented by subparallel reflection seismic facies, which have moderate to weak amplitudes and continuous reflections. Previous work has interpreted these facies as lacustrine background deposits (e.g., Dodd et al., 2019; Qin et al., 2021; Würtzen et al., 2022).

5. Characterization of lacustrine deltas and sub-lacustrine fans

5.1. Lacustrine deltaic clinothem stacking patterns

For the lacustrine deltaic clinothems in the lower succession of the study interval (the strata bounded to the bottom and top by T_3^m and MFS, respectively), the topset-to-foreset rollover trajectories (red arrows, Figs. 6, 7) were recognized through the topset-to-foreset rollover points (red dots, Figs. 6, 7). These deltaic clinothems are distinguishable by flat to steeply rising rollover trajectories that indicate progradational

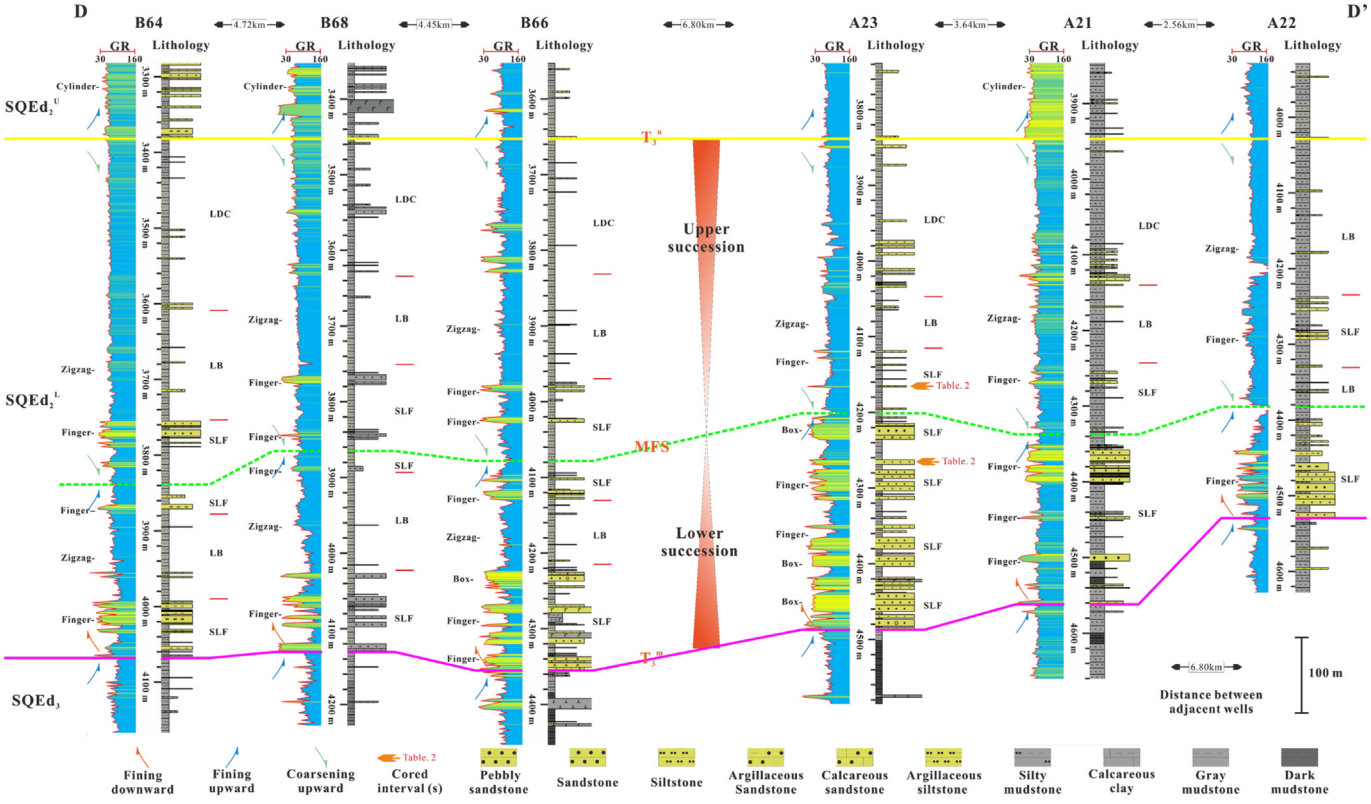

Fig. 5. Cross section of wells B64, B68, B66, A23, A21, and A22 showing sequence boundaries, well-log patterns (zigzag, finger, and box), and depositional systems of lacustrine deltaic clinothems (LDC), sub-lacustrine fans (SLF), and lacustrine background (LB) of SQEd_2^L in southwestern Bozhong Sag (D–D′, see location, Fig. 1C).

and aggradational stacking patterns (Figs. 6, 7). As such, the lacustrine deltaic clinothems in the lower succession of the study interval are referred to as "progradational to aggradational clinothem sets" (the concept of accommodation succession stacking based entirely on the geometric relationship of the strata. The PA clinothem sets correspond to the lowstand; Neal and Abreu, 2009; Neal et al., 2016; Paumard et al., 2019). Furthermore, the quantitative measurements suggest that PA clinothem sets have rollover trajectory angles (T_r) of 0.32°–1.07° (average 0.72°) and topset to bottomset thickness ratios (T_t/T_b) of 0.14–0.23 (average 0.18) (Table 2). Therefore, the PA clinothem sets have progradational and aggradational stacking patterns (the following progradational and aggradational stacking patterns are indicated by PA stacking patterns) with flat to steeply rising trajectories, steep rollover trajectory angles, greater bottomset thicknesses, and lower topset to bottomset thickness ratios (Table 2).

Corresponding rollovers have also been identified in the lacustrine deltaic clinothems in the upper succession of the study interval (the strata bounded at the bottom and top by the MFS and T_3^u, respectively). The specific trajectories of these deltaic clinothems are delineated by linking successive rollover points, as illustrated by the red arrows and blue dots in Figs. 6 and 7. These deltaic clinothems display slightly rising to flat and slightly falling rollover trajectories, indicating aggradational to progradational and degradational stacking patterns (Figs. 6, 7). We therefore designated these lacustrine deltaic clinothems in the upper succession of the study interval as "aggradational to progradational and degradational clinothem sets" (the concept of accommodation succession stacking based entirely on the geometric relationship of the strata. The APD clinothem sets correspond to the highstand; Neal and Abreu, 2009; Neal et al., 2016; Paumard et al., 2019). Quantitative measurements suggest that the APD clinothem sets have rollover trajectory angles (T_r) ranging from 0.18° to 1.01° (average 0.64°) and 'topset to bottomset thickness ratios' (T_t/T_b) ranging from 0.30 to 1.89 (average 0.99) (Table 2). APD clinothem sets are characterized by aggradational to progradational and degradational stacking patterns (the following aggradational to progradational and degradational stacking patterns are indicated by APD stacking patterns), which are associated with slightly rising to flat and slightly falling trajectories, relatively gentle rollover trajectory angles, thinner bottomsets, and higher topset to bottomset thickness ratios.

Our findings suggest that below the MFS of SQEd_2^L, lacustrine deltaic clinothems exhibit flat to steeply rising rollover trajectories with steep angles and smaller T_t/T_b ratios (Table 2). As such, the lower succession is made up of progradational and aggradational clinothem sets (PA clinothem sets) with progradational and aggradational stacking patterns (PA stacking patterns) (Figs. 6, 7). In contrast, the lacustrine deltaic clinothems above the MFS of SQEd_2^L consist of aggradational to progradational and degradational clinothem sets (APD clinothem sets) with slightly rising to flat and slightly falling rollover trajectories (Table 2). That is, the upper succession consists of APD clinothem sets associated with aggradational to progradational and degradational stacking patterns (APD stacking patterns) (Figs. 6, 7).

Meanwhile, thirty-four sets of lacustrine deltaic clinothems were measured to obtain a database of rollover trajectory angles (T_r), topset thickness (T_t), bottomset thickness (T_b), distance of progression (d_x), height of accretion (d_y), and topset to bottomset thickness ratio (T_t/T_b) (Table 2). Our results show that with rollover trajectory angles and the accretion height increasing, the thickness of the bottomset decreases significantly (Fig. 8A, B, and C), while the T_t/T_b ratios increase significantly (Fig. 8D). Recent studies also suggest that higher bottomset thickness, lower T_t/T_b ratios, and relatively gentle trajectory angles can be identified as contributing to greater efficiency of sediment delivery into deep-water systems (Zhang et al., 2019; Gong et al., 2019; Fisher et al., 2021). In contrast, in the lacustrine basin of this study, stratal stacking patterns of PA clinothem sets are characterized by flat to steeply rising rollover trajectories and steeper rollover trajectory angles than the counterpart of APD clinothem sets (Table 2). Meanwhile, these PA clinothem sets have a thicker bottomset and show more efficient sediment transport into deep-water sites

Table 1
Well logs, seismic facies, and core characteristics used in describing and interpreting the depositional styles in SQEd_2^1.

Depositional styles	Well-logging facies	Seismic facies (dip-view seismic sections)	RMS amplitude Attribute plan view	Core picture and grain size analysis	Interpretation
First depositional style	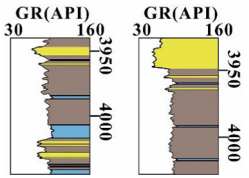	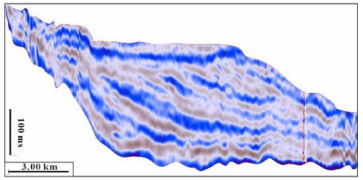	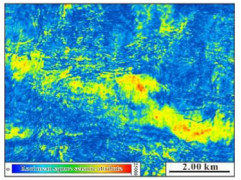	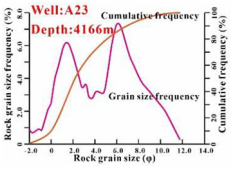	Lacustrine deltaic depositions
Second depositional style (in the upper succession)	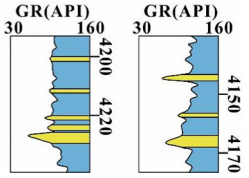	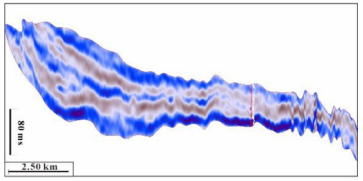	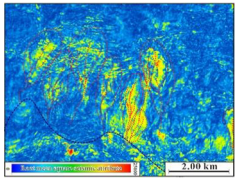	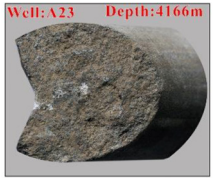	Sub-lacustrine fan deposits in the upper succession
Second depositional style (in the lower succession)	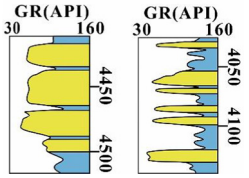	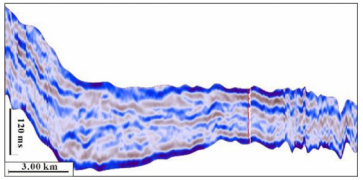	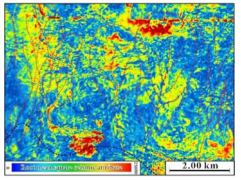	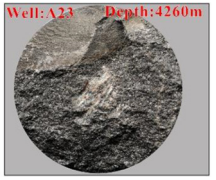	Sub-lacustrine fan deposits in the lower succession
Third depositional style	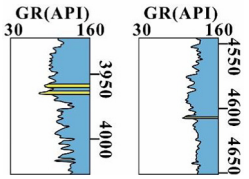	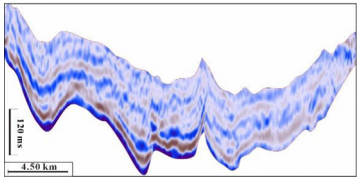	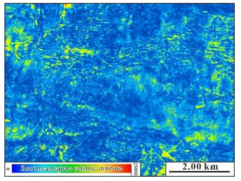	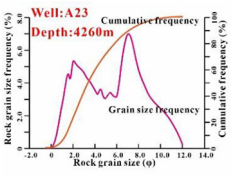	Lacustrine background deposits

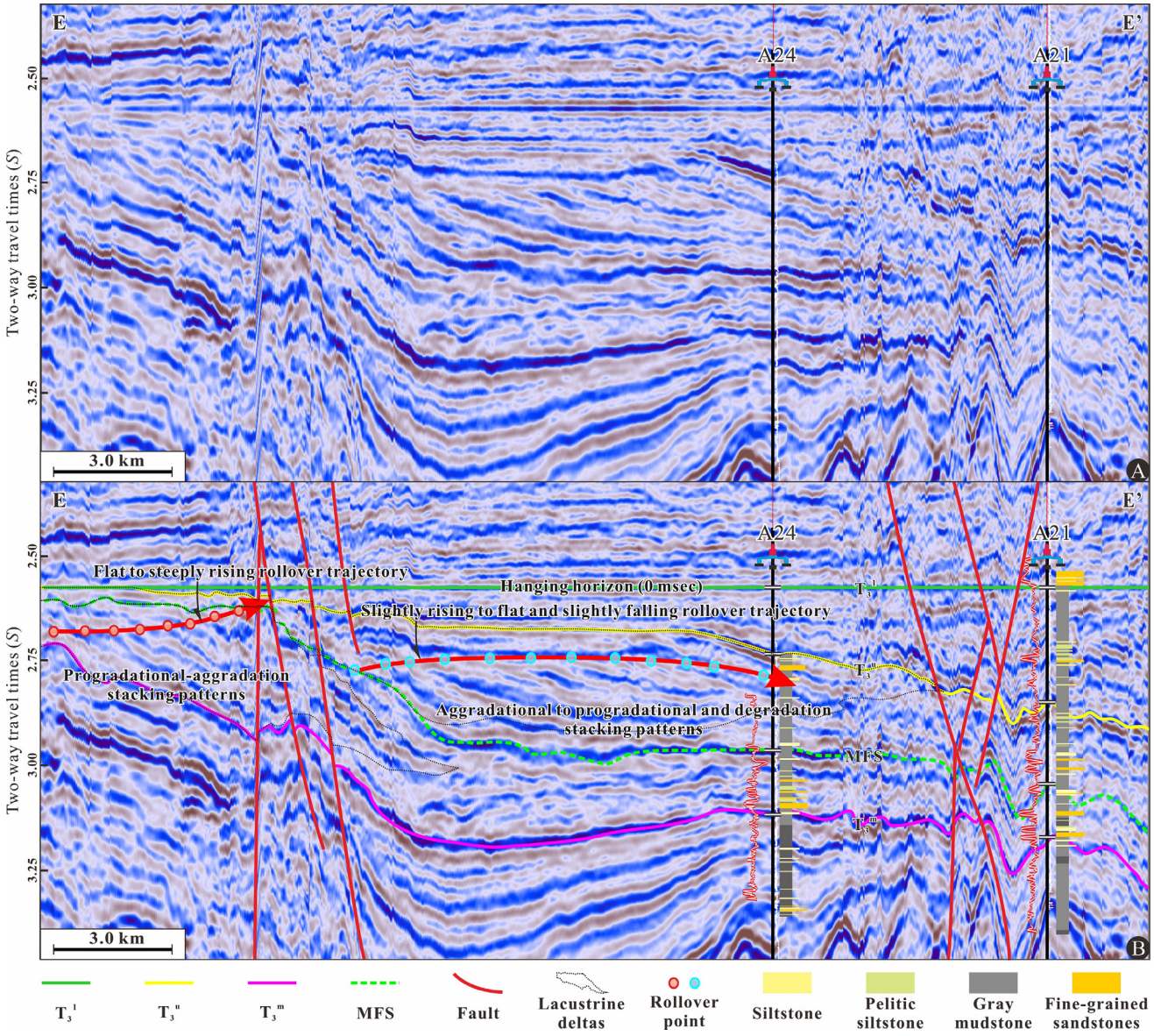

Fig. 6. Uninterpreted (A) and interpreted (B) regional 2D dip-oriented seismic profiles from the western segment of southwestern Bozhong Sag (E–E′, see location, Fig. 1C) showing the occurrence of two different types of the lacustrine deltaic clinothems with rollover points, trajectories, and stacking patterns. These seismic lines have been flattened by the T_3^l unconformity, dated at 27.4 Ma, in order to restore the paleohorizontal and original patterns of the documented rollover trajectories and deltaic clinothem stacking patterns.

(Fig. 8D). Results demonstrate opposing correlations between rollover trajectory angles and bottomset thickness in the southern Bozhong Sag.

5.2. Internal architecture of the sub-lacustrine fans

We characterized the internal architecture of deep-water fans using the morphology of their sedimentary composition (e.g., E. Liu et al., 2020; J. Liu et al., 2020). For the sub-lacustrine fans in the lower succession of the study interval (the strata bounded by T_3^m and MFS at the bottom and top, respectively), we initially identified their depositional boundaries and thicknesses using cross- and dip-view seismic sections of the sub-lacustrine fans (Fig. 9A, B). Subsequently, the sedimentary compositions of the sub-lacustrine fans were delineated by analyzing the typical root-mean-square (RMS) amplitude stratal slices and the thickness of the sedimentary systems (Fig. 10A, B). The sub-lacustrine fans of the lower succession exhibit channel–lobe systems with straight feeder channels and thick lobe complexes (Fig. 10C). Furthermore, these sub-lacustrine fans in the lower succession are up to 150 km^2 in area and a maximum thickness of ~400 m (averaging 210 m), the thickness increasing toward the center and gradually decreasing toward the periphery (Fig. 10A; Table 2).

In the sub-lacustrine fans of the upper succession (the strata bounded by MFS and T_3^u at the bottom and top, respectively), their corresponding depositional boundaries and thicknesses are also discernible from the cross- and dip-view seismic profiles of the sub-lacustrine fans (Fig. 9C, D). The specific sedimentary compositions of sub-lacustrine fans can be mapped through a comprehensive analysis of the thickness, the typical root-mean-square (RMS) amplitude stratal slices and the sandstone size of the deep-water depositional systems (Fig. 10D, E). Moreover, the architecture of sub-lacustrine fans in the upper succession also manifests as channel–lobe systems with sinuous feeder channels and thin lobe complexes (Fig. 10F). Quantitative measurements indicate that a single sub-lacustrine fan in the upper succession has an area of 60 km^2 and a maximum thickness of as much as 120 m (averaging 65 m), and its thickness increases toward the center and gradually decreases toward the periphery (Fig. 10D; Table 2).

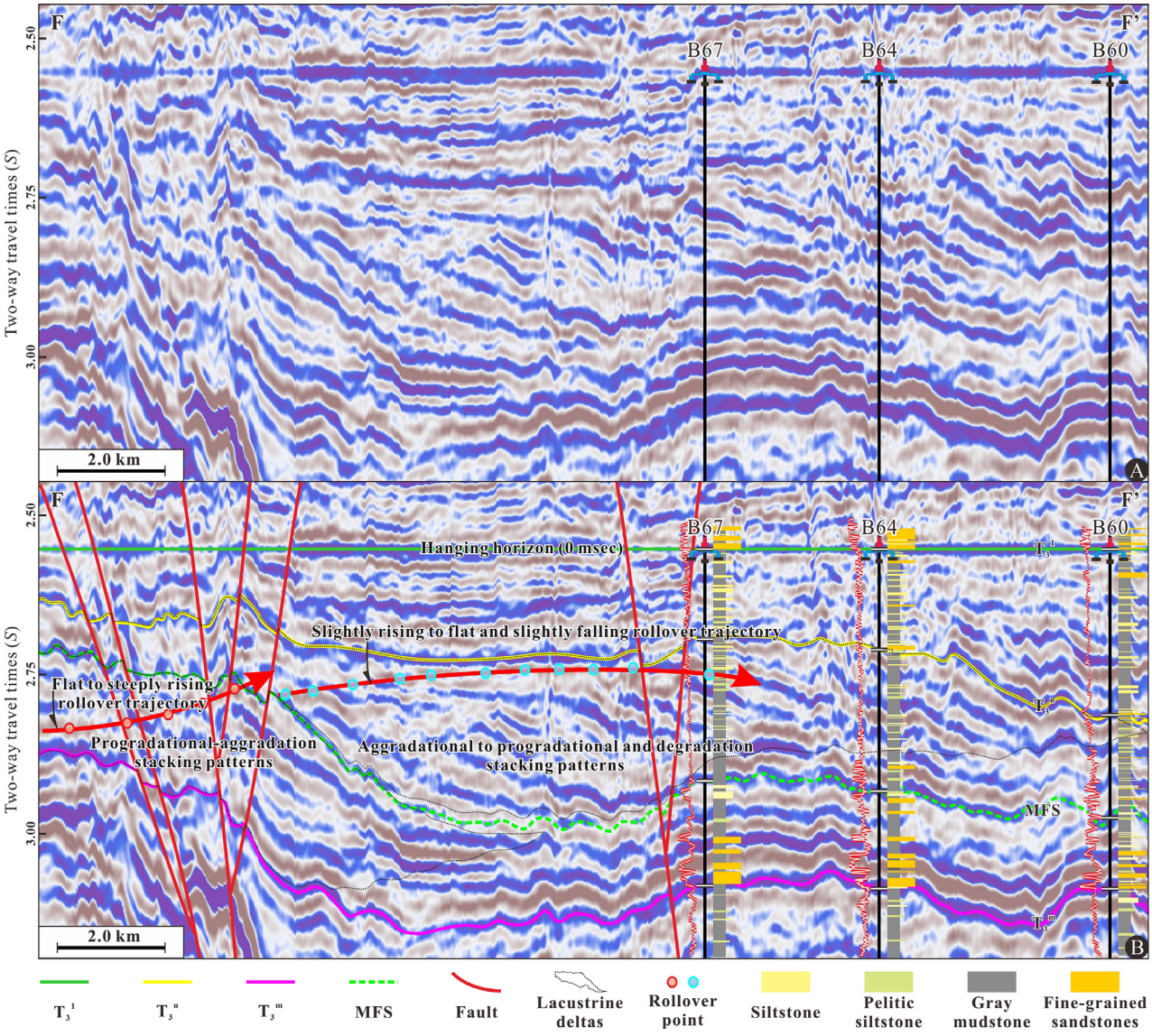

Fig. 7. Uninterpreted (A) and interpreted (B) regional 2D dip-oriented seismic profiles from the eastern segment of southwestern Bozhong Sag (F–F′, see location, Fig. 1C), showing the occurrence of two different types of lacustrine deltaic clinothems with rollover points, trajectories, and stacking patterns. The seismic lines shown have been flattened by the T_3^l unconformity, dated at 27.4 Ma, in order to restore the paleohorizontal and original patterns of the documented rollover trajectories and deltaic clinothem stacking patterns.

6. A deep time archive of paleoclimate

Previous studies have discussed that climate can influence the geochemical characteristics of sediments deposited in lacustrine environments by exerting control on exogenic processes and terrigenous sediment flux (Moradi et al., 2016). As a result, geochemical signals in sediments are heavily influenced climate during periods of sedimentation (Meng et al., 2012; Moradi et al., 2016; Qin et al., 2021). Therefore, elemental geochemical parameters and their ratios are widely utilized in paleoclimatic reconstructions (e.g., Moradi et al., 2016; Tao et al.,

Table 2
Statistics and comparison of the different architectures of clinothem stacking patterns and sub-lacustrine fans in SQEd_2^1.

Depositional systems	Architectures of the depositional systems	PA clinothem sets (the lower succession)	APD clinothem sets (the upper succession)
Lacustrine deltaic clinothems	Rollover trajectory angles (T_r)	0.32°–1.07°/0.72°	0.18°–1.01°/0.64°
	Topset thickness (T_t)	34.39 m–53.56 m/41.76 m	102.84 m–247.38 m/198.12 m
	Bottomset thickness (T_b)	174.12 m–270.77 m/232.27 m	107.46 m–342.61 m/211.14 m
	T_t/T_b	0.14–0.23/0.18	0.30–1.89/0.99
	Distance of progradation (d_x)	1.22 km–5.03 km/2.20 km	6.72 km–26.52 km/11.72 km
	Height of accretion (d_y)	11.71 m–57.92 m/34.12 m	57.98 m–283.38 m/143.17 m
	Rollover trajectories	Flat to steeply rising	Slightly rising to flat and slightly descending
	Stacking patterns	Progradational and aggradational	Aggradational to progradational and degradational
Sub-lacustrine fans	Sedimentary compositions of sub-lacustrine fans	Straight feeder channels and thick lobe complexes	Sinuous channels and thin lobe complexes
	The scale of sub-lacustrine fans	Average thickness: 210 m Area: more than 150 km^2	Average thickness: 65 m Area: more than 60 km^2

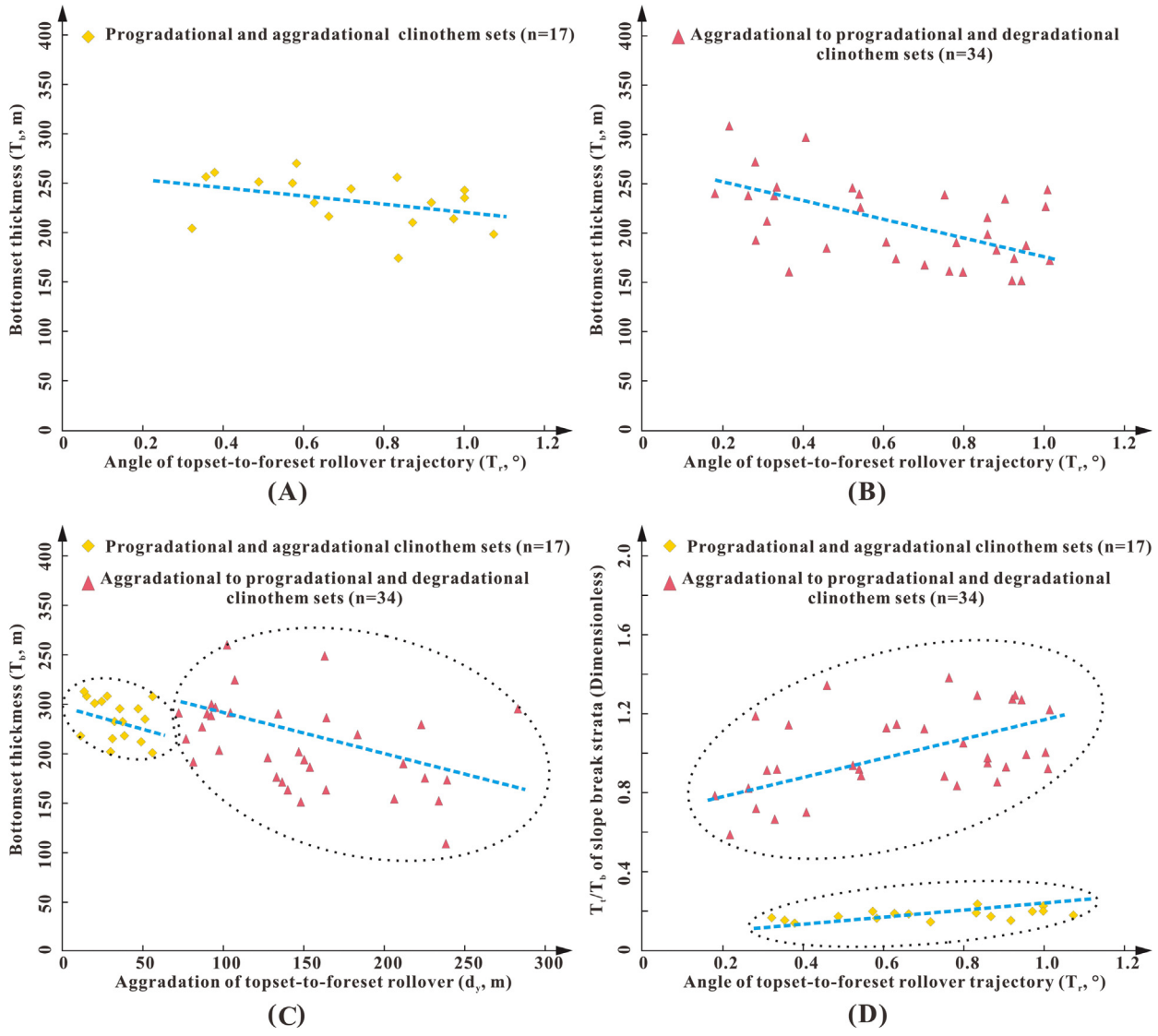

Fig. 8. Plots showing distinctive rollover trajectory angles with bottomset thickness (A, B) and accretion height (C). Rollover trajectory angles with topset to bottomset thickness ratios (D) of the PA and APD clinothem sets. As the rollover trajectory angles and the accretion height increase, the bottomset thickness decreases significantly, and T_t/T_b ratios increase significantly.

2017; Qin et al., 2021). In addition, extensive research has been conducted on the geochemical properties and formation conditions of the source rocks in the southwestern Bozhong Sag, resulting in a substantial database of geochemical archives in the Dongying Formation. Notably, 135 sets of major and trace elements, as well as their ratios, from mudstone samples collected from four members of the Dongying Formation (E_3d_1, $E_3d_2^U$, $E_3d_2^L$, and E_3d_3) in southwestern Bozhong Sag, as presented in Yang et al. (2021), are of excellent value for reconstructing paleoclimatic fluctuations. In this investigation, a total of 42 assemblages of trace elements, major elements, and their respective ratios associated with SQEd_2^L have been extracted from the dataset mainly provided by Yang et al. (2021). Out of these, 22 assemblages are attributed to the upper succession of SQEd_2^L, while the remaining 20 assemblages pertain to the lower succession of SQEd_2^L. In this investigation, the ratios of major elements and trace elements (e.g., *Cu/Sr*, *Ca/Mg*, *U/Th*, *Co/Fe*, and *C*-value) were employed to qualitatively assess the variations in these geochemical indicators within the upper and lower successions of the SQEd_2^L. This analysis aims to provide insights into the deep-time paleoclimate fluctuations that occurred during the sedimentary phase of the SQEd_2^L.

As illustrated in Fig. 11, the *Cu/Sr*, *Ca/Mg*, *U/Th*, and *Co/Fe* ratios and *C*-value exhibit comparatively higher values in the lower succession of SQEd_2^L compared to the upper succession. This observation indicates that the different paleoclimatic phases were most likely present in the SQEd_2^L. In general, the copper (*Cu*)/strontium (*Sr*) ratio is a crucial paleoclimatic indicator. A high *Cu/Sr* ratio is indicative of a warm and humid climate, whereas a low *Cu/Sr* ratio is indicative of a hot and dry paleoclimate (Awan et al., 2020). Similarly, the *C*-value has demonstrated utility as a paleoclimatic indicator of moist versus arid sedimentary conditions, where *C*-value = Σ (*Fe*, *Mn*, *Cr*, *Ni*, *V*, *Co*) / Σ (*Ca*, *Mg*, *Sr*, *Ba*, *K*, *Na*) (Moradi et al., 2016; Awan et al., 2020). During moist conditions, elements like *Ca*, *Mg*, *Sr*, *Ba*, *K*, and *Na* exist in higher concentration whereas in arid conditions, saline minerals containing *Ca*, *Mg*, *Sr*, *Ba*, *K*, and *Na* precipitate more readily (Moradi et al., 2016).

In lacustrine systems, the precipitation rate of iron (*Fe*) is relatively higher than that of cobalt (*Co*) (Awan et al., 2020; Yang et al., 2021). However, with increasing water depth, the concentration of *Co* gradually increases (Yang et al., 2015). Due to this, the *Co/Fe* ratio has been used to indicate the water depth in sedimentary environments (Yang et al., 2021). A high *Co/Fe* ratio indicates a relatively deep-water sedimentary environment whereas a lower *Co/Fe* ratio denotes shallowing of the water column. Additionally, low uranium (*U*)/thorium (*Th*) ratios often occur in reduced sediments (Wignall and Twitchett, 1996). The lower succession of SQEd_2^L is characterized by alternating oxidizing

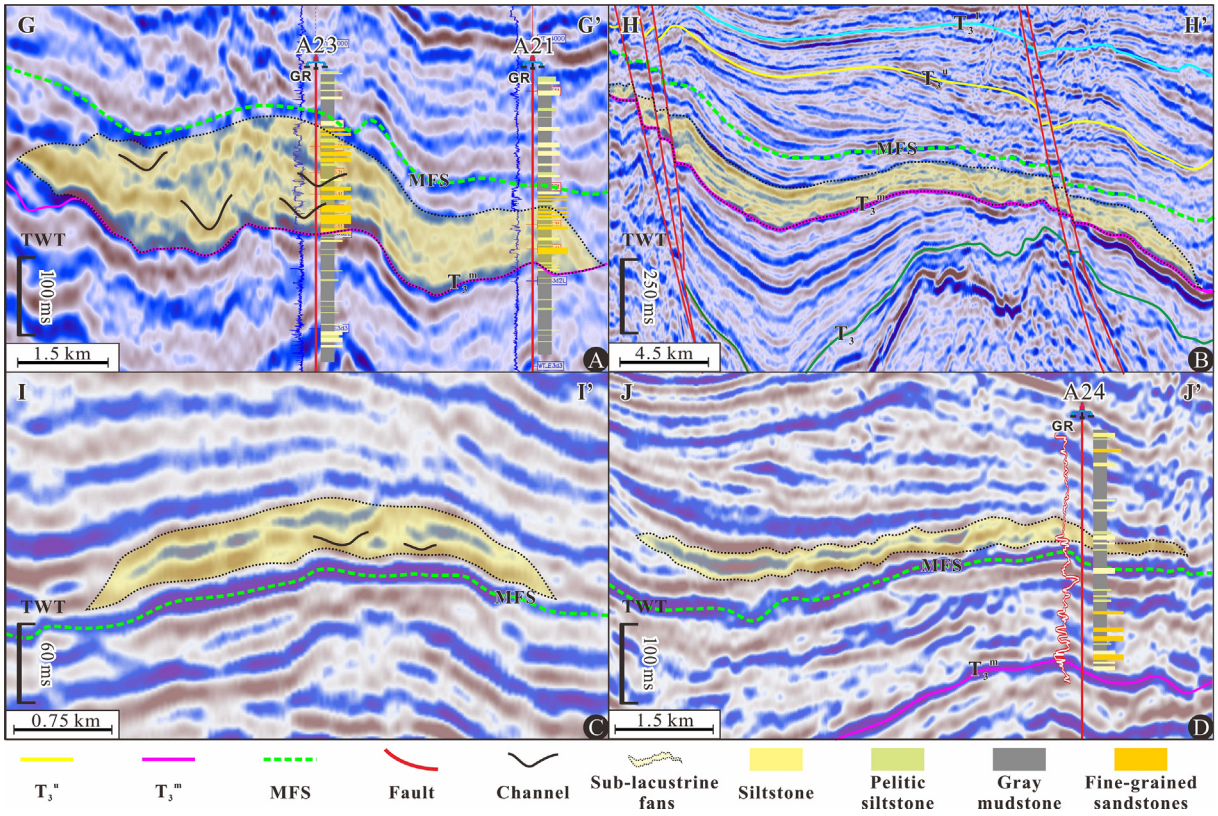

Fig. 9. Cross-view (A) and dip-view (B) seismic transects (G–G′ and H–H′, see location, Fig. 1C) showing the characteristics of the larger channel–lobe systems in the lower succession. Cross-view seismic transect (C) and dip-view (D) seismic transect (I–I′ and J–J′, see location, Fig. 1C) showing the characteristics of the smaller channel–lobe systems in the upper succession (see location, Fig. 1C).

and reducing conditions and the upper succession is dominated by oxidizing conditions. Finally, high calcium (*Ca*)/magnesium (*Mg*) ratios are generally associated with high evaporation rates and saline conditions, whereas low *Ca*/*Mg* ratios denote lower salinity conditions (Qin et al., 2021).

These results indicate a relative humid climate with extensive deep-water environments and reducing conditions during the lower succession of SQEd_2^L and a comparatively semi-arid climate with oxidizing condition during the upper succession of SQEd_2^L.

7. Discussion

7.1. Delta-to-fan sediment connectivity in lacustrine basins

Previous studies about the Neogene Lake Pannon, the Northern South China Sea Margin, and the Eocene Dongying Depression of the Bohai Bay Basin have demonstrated that the alternating stacking patterns of clinothems are associated with the delivery of relative amounts of terrigenous sediment to deep-water sites (e.g., Sztanó et al., 2013; Gong et al., 2015a; Paumard et al., 2019; E. Liu et al., 2020; J. Liu et al., 2020). In marine basins, such as the Lower Cretaceous (Albian) strata in the Alaska North Slope, the Late Miocene–Early Pliocene prograding shelf system (Molo Formation) offshore Norway, and the Late Miocene–Quaternary strata in the northwestern South China Sea Margin, progradational to aggradational (PA) deltaic clinothems with rising trajectories are rarely associated with submarine fans, whereas those with aggradational to progradational and degradational (APD) deltaic clinothems and flat to slightly falling trajectories often produce large-scale submarine fans (e.g., Henriksen et al., 2009, 2011a; Gong et al., 2015b). In contrast, in lacustrine settings, the PA clinothem sets are characterized by thick bottomset, whereas the APD clinothem sets lack evidence of bottomset in the Eocene Dongying Depression (e.g., E. Liu et al., 2020; J. Liu et al., 2020). However, our investigation of the Oligocene Bozhong Sag reveals that the APD clinothem sets also exhibit a small-scale bottomset (Fig. 12), which was also reported in the Eocene Shahejie Formation of Dongying Sag, Bohai Bay Basin (Yang et al., 2023b). The bottomsets of deltaic clinothems are commonly associated with deep-water deposition, such as deep-water fans (e.g., Gong et al., 2015a; E. Liu et al., 2020; J. Liu et al., 2020; Wu et al., 2022). This indicates that above the MFS, the terrigenous sediments were also transported and dispersed into the deep-lacustrine basin floors and formed the sub-lacustrine fans with channel–lobe systems.

The most direct evidence for a coupled delta–fan system is observable, synchronous deposition between deltas and fans (Qi et al., 2023). As lake/sea level rises or falls, there are distinct similarities in the stacking patterns and trajectories of lacustrine deltaic clinothems and shelf-edge deltaic clinothems. However, the contemporaneous deep-water fans in the basin floor show significant differences between marine and lacustrine systems (Gong et al., 2015a, 2015b, 2019, Gong et al., 2019; Paumard et al., 2019; E. Liu et al., 2020; J. Liu et al., 2020). Specifically, during the lake/sea level rising stage, both lacustrine deltaic clinothems in lacustrine systems and shelf-edge deltaic clinothems in marine systems display a progradational to aggradational (PA) stacking pattern, along with flat to rising trajectories. In this stage, large-scale sub-lacustrine fans form on the lacustrine basin floor, while submarine fans are rarely found on the marine basin floor (Gong et al., 2019; Paumard et al., 2019) (Fig. 13A). Conversely, during the lake/sea level falling stage, both lacustrine deltaic clinothems in lacustrine systems and shelf-edge deltaic clinothems in marine systems exhibit an aggradational to progradational and degradational (APD) stacking pattern, and the trajectories shift from rising to flat and descending. It is noteworthy that in this stage, small-scale sub-lacustrine fans develop

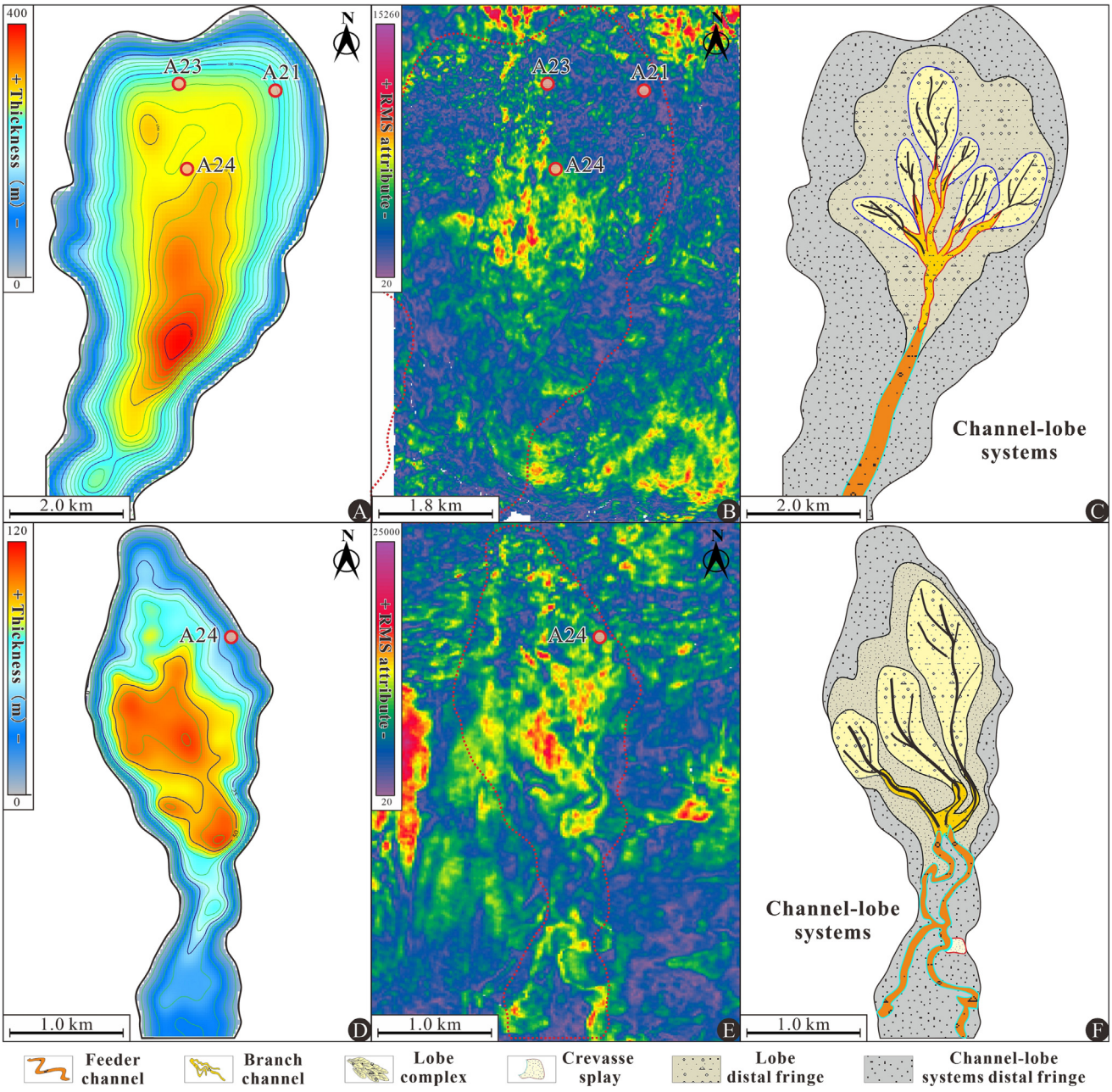

Fig. 10. Architectures of thickness (A), the typical root-mean-square (RMS) amplitude stratal slices (B), and sedimentary composition (C) of sub-lacustrine channel–lobe systems show that larger sub-lacustrine fans in the lower succession have straight channels and thick lobe complexes (orange box, see location, Fig. 1C). Architectures of thickness (D), the typical root-mean-square (RMS) amplitude stratal slices (E), and sedimentary composition (F) of sub-lacustrine channel–lobe systems show that smaller sub-lacustrine fans in the lower succession have sinuous channels and thin lobe complexes (green box, see location, Fig. 1C).

in the lacustrine basin floor, whereas large-scale submarine fans form in the marine basin floor (Gong et al., 2019; Yang et al., 2023b) (Fig. 13B). Meanwhile, it is illustrated that the deep-lacustrine sedimentary processes and products in the lake-level rising stage (corresponding APD clinothem sets) exhibit similarities compared to their counterparts in the lake-level falling stage (corresponding PA clinothem sets) in the lacustrine basins (Fig. 13).

Observably, in the lacustrine basins of our study, we observe the opposite relationship with marine basins. PA deltaic clinothems with flat to steeply rising rollover trajectories are coupled with large-scale deep-water fans featuring straight channels and thick lobes (Figs. 12, 13). APD deltaic clinothems with slightly rising to flat and slightly falling rollover trajectories are coupled with small-scale deep-water fans characterized by sinuous channels and thin lobes (Figs. 12, 13).

7.2. Climate-driven, supply-dominated deep-lacustrine depositional model

This observed relationship adds to the growing body of evidence demonstrating a reversal of conventional stratigraphic architectures between marine and lacustrine settings (Bohacs et al., 2000; Gong et al., 2019; Zhang et al., 2020; Gearon et al., 2022). This discrepancy in sediment partitioning between deltas and deep-water fans is due to several factors. Along continental margins, the shelf edge plays a crucial role in modulating sediment transport to the basin floor. The cases from Karoo Basin, the northwestern South China Sea margin, and the Middle Miocene Pearl River margin demonstrate that sediment accumulation at the shelf edge signifies the initiation of terrestrial sediment delivery to deep-water sites, which is then followed by the transportation and dispersal of sediment from the shelf edge to the basin floor (Henriksen

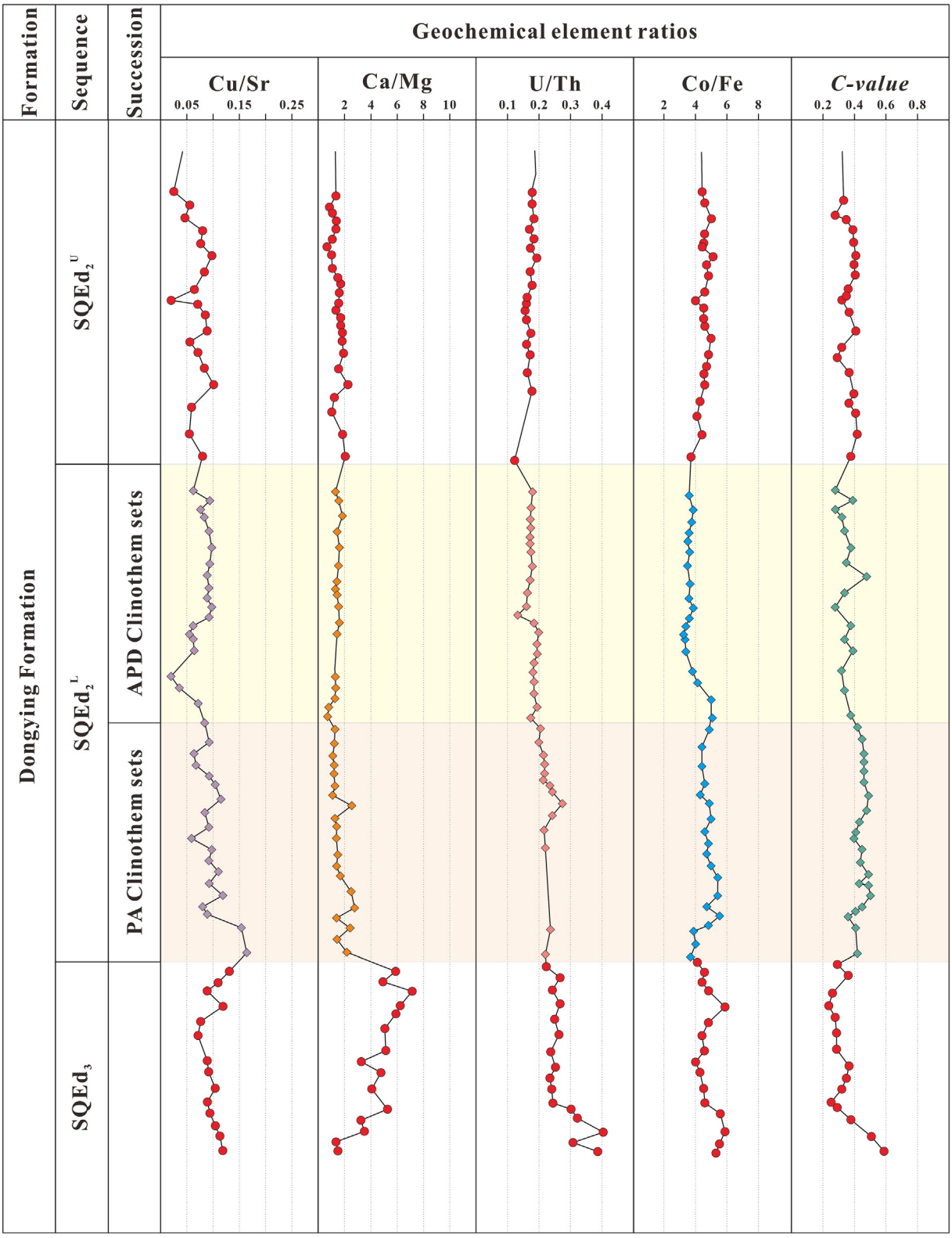

Fig. 11. Distribution and evolution of the geochemical elements and their ratios in the mudstones of the Dongying Formation in southwestern Bozhong Sag (original data from Yang et al., 2021). Elemental geochemical parameters and their ratios can be utilized to reconstruct the sedimentary paleoenvironment. The PA clinothem sets have higher values of *Cu/Sr*, *Cg/Mg*, *U/Th*, *Co/Fe*, and *C*-value, indicating the sedimentary paleoenvironment of humid climate cycles, deeper water depth, and lower ambient water salinity. In contrast, the APD clinothem sets have lower values of *Cu/Sr*, *Cg/Mg*, *U/Th*, *Co/Fe*, and *C*-value, indicating semiarid climate cycles, some oxidation, and increased ambient water salinity.

et al., 2009; Dixon et al., 2012; Gong et al., 2019, 2021). Conversely, in lacustrine basins, riverine sediments can easily traverse the slope break via hyperpycnal flow. The cases from the Lower Cretaceous, Neuquén Basin, and Eocene Dongying Sag of the Bohai Bay Basin certify that large volumes of sediment are transported and dispersed onto the lacustrine basin floor (Zavala and Arcuri, 2016; E. Liu et al., 2020; J. Liu et al., 2020; Yang et al., 2023a, 2023b). The distinct geomorphological differences between the ramp-style deltaic clinothems in lacustrine

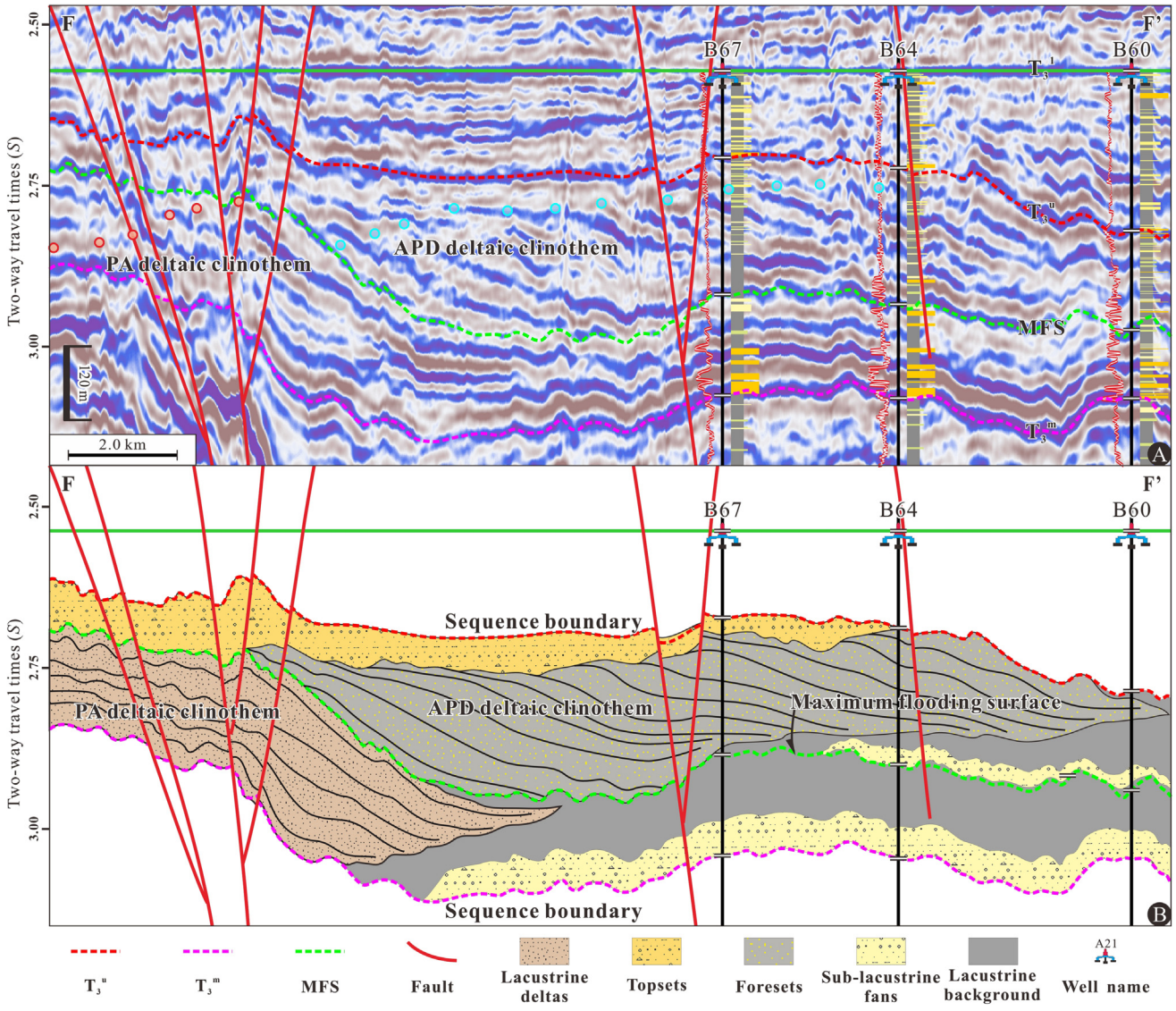

Fig. 12. Two-dimensional model diagram illustrating the sediment connectivity between lacustrine deltaic clinothem stacking patterns and sub-lacustrine fans, and the dispersal of terrigenous sediments into the deep-lacustrine. (A) Dip-view seismic section tied to well logs and lithology shows the stacking pattern and rollover trajectories of lacustrine deltaic clinothems. (B) According to the seismic profiles, well-logging data, and sedimentary system analysis, the corresponding relationships are as follows: The PA clinothem sets have transported and dispersed more sediments into deep water, and the larger sub-lacustrine fans are coupled with progradational and aggradational stacking patterns; the APD clinothem sets have transported and dispersed less sediment into deep water and the smaller sub-lacustrine fans are coupled with aggradational to progradational and degradational stacking patterns.

basins and the shelf-edge deltaic clinothems in marine basins have a profound impact on the sedimentary processes involved in the dispersal of terrigenous sediments into deep-water sites (Gong et al., 2019; E. Liu et al., 2020; J. Liu et al., 2020). In lacustrine basins, sediments can be more easily captured by sub-lacustrine channels and more efficiently delivered onto the lacustrine basin floor due to their smaller size and connectively delta-to-fan sedimentary processes compared to those of marine basins (Bahka et al., 2017; Gong et al., 2019; E. Liu et al., 2020; J. Liu et al., 2020).

Furthermore, previous studies on Early Eocene successions from Spitsbergen and offshore Ireland, the Neogene Lake Pannon, and the South China Sea have demonstrated that sea-level eustasy and sediment supply jointly control the growth of deltaic clinothems and deep-water fans (Johannessen and Steel, 2005; Sztanó et al., 2013; Lin et al., 2018). The transgressive–regressive shifts of the shelf-edge and shoreline are controlled by base-level and sediment supply, leading to the formation of distinct trajectories and clinothem geometries (Catuneanu, 2019; Sømme et al., 2009; Zhang et al., 2019). On the other hand, previous studies have demonstrated that the main reason for the marked contrast in sediment partitioning across marine versus lacustrine clinoforms is climate (Gong et al., 2019; Zhang et al., 2019; Gearon et al., 2022). As a result, fluctuations in lake level and sediment supply are much more sensitive to local climatic signatures in closed lake basins compared to the jointly controlled factors of sea level eustasy and sediment supply in marine basins (Gong et al., 2019; Zhang et al., 2019; Gearon et al., 2022). Meanwhile, previous studies from ancient lacustrine basins in the Oligocene Qikou Sag and Eocene Dongying Sag of the Bohai Bay Basin and modern lake basins, Poyang Lake in China and Lake Eyre in Australia, have revealed that fluctuations in lake levels and sediment supply are predominantly driven by a highly variable climate on shorter time scales ($SQE_{d_2^L}$ spans a time interval of much less than 2.9 Myr) (Croke et al., 1996; Hui et al., 2008; Yu et al., 2021; Qin et al., 2021). Changes in climatic signatures can directly influence variations in river discharge, sediment–water flux, precipitation, and evaporation, which further affect lake-level fluctuation (Zavala and Arcuri, 2016; Gong et al., 2019; E. Liu et al., 2020; J. Liu et al., 2020; Wu et al., 2022). River energy, sediment concentration, and ambient water salinity also fluctuate periodically with climatic

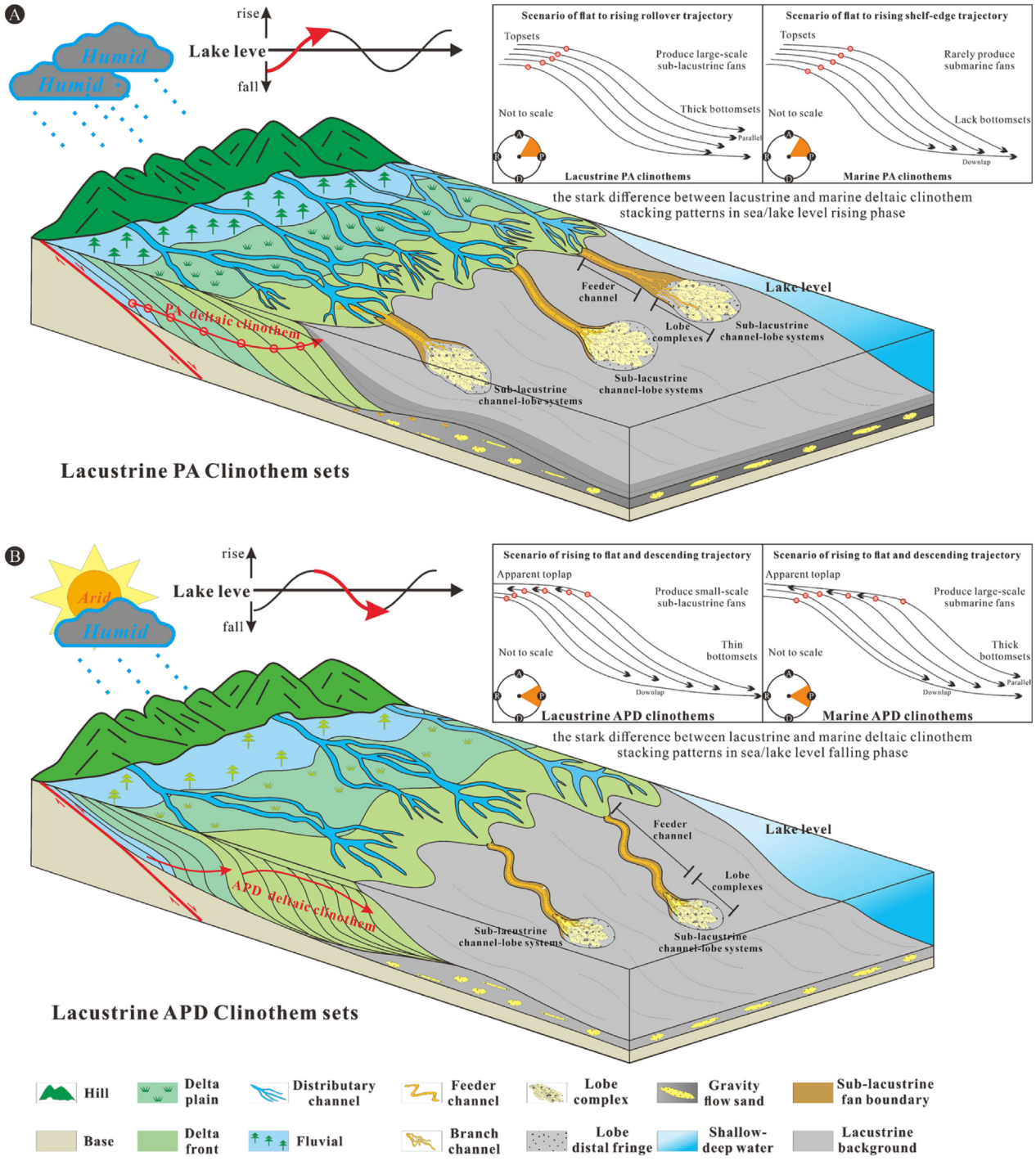

Fig. 13. 3D deep-lacustrine depositional models and the stark differences between lacustrine and marine deltaic clinothems reveal sediment connectivity between lacustrine deltas and deep-water fans, which is dominated by sediment-supply and driven by semiarid to humid climate forcing. (A) During humid climatic cycles, heightened river discharge and sediment–water flux lead to relative lake-level rise. Lacustrine deltaic clinothems, characterized by progradational and aggradational stacking, are coupled with large-scale sub-lacustrine fans with straight feeder channels and thick lobe complexes. (B) During semiarid climatic cycles, reduced river discharge and sediment–water flux cause lake levels to fall. Lacustrine deltaic clinothems are characterized by aggradational to progradational and degradational stacking patterns, coupled with small-scale sub-lacustrine fans with sinuous feeder channels and thin lobe complexes.

cycles (Gong et al., 2019). As a result, the fluctuation of sediment supply caused by climate forcing can be considered the dominant factor controlling the characteristics of lacustrine deltaic clinothems and the architecture of sub-lacustrine fans at SQEd^{L}_{2}.

Geochemical indicators of the lower and upper successions of SQEd^{L}_{2} indicate that PA clinothem sets are linked to relatively humid climate cycles, whereas APD clinothem sets are associated with generally semiarid climate cycles (Fig. 11). The climate forcing of the arid–humid cycle can greatly affect various aspects of lake environments, such as river discharge, sediment–water flux, precipitation, and evaporation (Blum and Törnqvist, 2000; Shankman et al., 2006; Gong et al., 2019). This phenomenon is further reflected in variations of lake-level fluctuation, lacustrine deltaic clinothem stacking patterns, and relative amounts of sediment delivery into the deep-lake floor via feeder

channels (Zavala and Arcuri, 2016; E. Liu et al., 2020; J. Liu et al., 2020; Yang et al., 2023a). More specifically, in humid climate cycles, increased river discharge, sediment–water flux, and precipitation lead to lake-level rises (Gong et al., 2019; J. Liu et al., 2020; Wu et al., 2022). This phenomenon gives rise to PA stacking patterns in lacustrine deltaic clinothems. Furthermore, increased river energy and sediment concentrations, combined with freshwater conditions (Fig. 11), promote the dispersal of large-scale sediments into deep-lacustrine systems. This is manifested in the architecture of straight feeder channels and thicker lobe complexes (Figs. 10C, 13A). Conversely, during semiarid climate cycles, river discharge decreases and evaporation increases, causing the lake level to fall. This phenomenon results in APD stacking patterns in lacustrine deltaic clinothems. Additionally, reduced river energy and sediment concentration, as well as increased ambient water salinity (Fig. 11), give rise to small-scale sediment amounts being transported into the lacustrine basin floor through sinuous feeder channels (Figs. 10F, 13B).

Therefore, the coupling relationship between deltaic clinothem stacking patterns and sub-lacustrine fans in humid climate cycles indicates more efficient sediment dispersal into deep-water sites. That is, increased sediment connectivity between deltas and deep-water fans during humid climate cycles in the Oligocene southwestern Bozhong Sag (Fig. 13).

8. Conclusions

Subsurface data from the Oligocene southwestern Bozhong Sag reveal that both lacustrine deltaic clinothems and outlying sub-lacustrine fans were developed in the lower succession and upper succession of SQEd_2^L. During the humid climate cycle, lacustrine deltaic clinothems are characterized by progradational to aggradational (PA) stacking patterns and flat to steeply rising rollover trajectories in the lower succession, whereas during the semiarid climatic cycle, lacustrine deltaic clinothems are dominated by aggradational to progradational and degradational (APD) deltaic clinothems and slightly rising to flat and slightly falling rollover trajectories in the upper succession.

The sediment connectivity between lacustrine deltaic clinothems and coeval outlying sub-lacustrine fans in Bozhong Sag (APD lacustrine deltaic clinothems produce small-scale deep-water fans characterized by sinuous channels and thin lobes, whereas PA lacustrine deltaic clinothems produce large-scale deep-water fans characterized by straight channels and thick lobes) is directly opposite to the marine-style (PA shelf-edge deltaic clinothems rarely produce deep-water fans, whereas APD shelf-edge deltaic clinothems produce large-scale deep-water fans). The main reason for the marked contrast in sediment partitioning across marine versus lacustrine clinoforms is climate. The catchment dynamics of the closed lake basin are more sensitive to regional climate conditions compared to marine systems.

The depositional model of deep-lacustrine systems, driven by climate dynamics and dominated by sediment supply, is employed to rationalize the increased sediment connectivity between deltas and deep-water fans within deep-lacustrine systems. Specifically, sediment transport and dispersion between deltas and deep-water fans are more efficient during humid climatic cycles. Conversely, during semiarid climate cycles, sediment connectivity between deltas and deep-water fans is relatively muted.

CRediT authorship contribution statement

Puyu Liu: Writing – original draft, Writing – review & editing. **Chenglin Gong:** Conceptualization, Supervision, Writing – review & editing. **James H. Gearon:** Conceptualization, Methodology, Writing – review & editing. **Dayong Guan:** Formal analysis, Software. **Qiming Wang:** Software. **Kun Qi:** Conceptualization, Writing – review & editing. **Dongwei Li:** Software.

Data availability

Data will be made available on request.

Declaration of competing interest

We declare that we have no financial and personal relationships with other people or organizations that can inappropriately influence our work.

Acknowledgments

We would like to sincerely thank Editor Dr. Catherine Chagué, Dr. Jörg Lang, and an anonymous reviewer for their careful review, constructive comments, and assistance, which have significantly improved the manuscript, and Parthiban Rajendran for handing over our manuscript. We also gratefully thank the Tianjin Branch of CNOOC and the Bohai Petroleum Research Institute for providing the data and for their permission to publish the results of this study. Additionally, we extend our appreciation to Dr. Amanda Masterson for her invaluable assistance in refining the English-language aspects of our manuscript. This study was financially funded by the Tianjin Branch of the China National Offshore Oil Corporation-China University of Petroleum (Beijing) Strategic Cooperation Science and Technology Project (CCL2020TJX0NST1276).

References

Awan, R.S., Liu, C., Gong, H., Dun, C., Tong, C., Chamssidini, L.G., 2020. Paleo-sedimentary environment in relation to enrichment of organic matter of Early Cambrian black rocks of Niutitang Formation from Xiangxi area China. Marine and Petroleum Geology 112, 104057. https://doi.org/10.1016/j.marpetgeo.2019.104057.

Bahka, J., Kang, N.K., Yi, B., Lee, S., Jeong, S., Urgeles, R., Yoo, D., 2017. Sedimentary characteristics and processes of submarine mass-transport deposits in the Ulleung Basin and their relations to seismic and sediment physical properties. Marine Geology 393, 124–140.

Blum, M.D., Törnqvist, T.E., 2000. Fluvial responses to climate and sea-level change: a review and look forward. Sedimentology 47 (Suppl. 1), S2–S48.

Bohacs, K.M., Carroll, A.R., Neal, J.E., Mankiewicz, P.J., 2000. Lake-basin type, source potential, and hydrocarbon character: an integrated-sequence-stratigraphic-geochemical framework. In: Gierlowski-Kordesch, E.H., Kelts, K.R. (Eds.), Lake Basins Through Space and Time. American Association of Petroleum Geologists Studies in Geology, pp. 3–34.

Carroll, A.R., Bohacs, K.M., 1999. Stratigraphic classification of ancient lakes: balancing tectonic and climatic controls. Geology 27, 99–102.

Catuneanu, O., 2019. Model-independent sequence stratigraphy. Earth-Science Reviews 188, 312–388.

Chen, H., Wood, L.J., Gawthorpe, R.L., 2021. Sediment dispersal and redistributive processes in axial and transverse deep-time source-to-sink systems of marine rift basins: Dampier Sub-basin, Northwest Shelf, Australia. Basin Research 33, 227–249.

Coe, M.T., Birkeet, C.M., 2004. Calculation of river discharge and prediction of lake height from satellite radar altimetry: example for the Lake Chad basin. Water Resources Research 40, W10205. https://doi.org/10.1029/2003WR002543 (2004).

Covault, J.A., Normark, W.R., Romans, B.W., Graham, S.A., 2007. Highstand fans in the California borderland: the overlooked deep-water depositional systems. Geology 35, 783–786.

Croke, J., Magge, J., Price, D., 1996. Major episodes of Quaternary activity in the lower Neales River, northwest of Lake Eyre, central Australia. Palaeogeography Palaeoclimatology Palaeoecology 124, 1–15.

Dixon, J.F., Steel, R.J., Olariu, C., 2012. River-dominated, shelf-edge deltas: delivery of sand across the shelf break in the absence of slope incision. Sedimentology 59, 1133–1157.

Dodd, T.J.H., McCarthy, D.J., Richards, P.C., 2019. A depositional model for deep-lacustrine, partially confined, turbidite fans: Early Cretaceous, North Falkland Basin. Sedimentology 66, 53–80.

Feng, Y., Jiang, S., Hu, S., Li, S., Lin, C., Xie, X., 2016. Sequence stratigraphy and importance of syndepositional structural slope-break for architecture of Paleogene syn-rift lacustrine strata, Bohai Bay Basin, E. China. Marine and Petroleum Geology 69, 183–204.

Fisher, W.L., Galloway, W.E., Steel, R.J., Olariu, C., Kerans, C., Mohrig, D., 2021. Deep-water depositional systems supplied by shelf-incising submarine canyons: recognition and significance in the geologic record. Earth-Science Reviews 214, 103531. https://doi.org/10.1016/j.earscirev.2021.103531.

Fongngern, R., Olariu, C., Steel, R.J., Krézsek, C., 2016. Clinoform growth in a Miocene, Paratethyan deep lake basin: thin topsets, irregular foresets and thick bottomsets. Basin Research 28, 770–795.

Fongngern, R., Olariu, C., Steel, R.J., Mohrig, D., Krézsek, C., Hess, T., 2018. Subsurface and outcrop characteristics of fluvial-dominated deep-lacustrine clinoforms. Sedimentology 65, 1447–1481.

Gearon, J.H., Olariu, C., Steel, R.J., 2022. The supply-generated sequence: a unified sequence-stratigraphic model for closed lacustrine sedimentary basins with evidence

from the Green River Formation, Uinta Basin, Utah, U.S.A. Journal of Sedimentary Research 92, 813–835.
Gong, C., Wang, Y., Pyles, D.R., Steel, R.J., Xu, S., Xu, Q., Li, D., 2015a. Shelf-edge trajectories and stratal stacking patterns: their sequence-stratigraphic significance and relation to styles of deep-water sedimentation and amount of deep-water sandstone. American Association of Petroleum Geologists Bulletin 99, 1211–1243.
Gong, C., Wang, Y., Steel, R.J., Olariu, C., Xu, Q., Liu, X., Zhao, Q., 2015b. Growth styles of shelf-margin clinoforms: prediction of sand- and sediment-budget partitioning into and across the shelf. Journal of Sedimentary Research 85, 209–229.
Gong, C., Sztanó, O., Steel, R.J., Xian, B., Galloway, W.E., Bada, G., 2019. Critical differences in sediment delivery and partitioning between marine and lacustrine basins: a comparison of marine and lacustrine aggradational to progradational clinothem pairs. Geological Society of America Bulletin 131, 766–781.
Gong, C., Li, D., Steel, R.J., Peng, Y., Xu, S., Wang, Y., 2021. Delta-to-fan source-to-sink coupling as a fundamental control on the delivery of coarse clastics to deepwater: insights from stratigraphic forward modelling. Basin Research 33, 2960–2983.
Haq, B.U., Hardenbol, J., Vail, P.R., 1987. Chronology of fluctuating sea levels since the Triassic. Science 235, 1156–1167.
Henriksen, S., Hampson, G.J., Helland-Hansen, W., Johannessen, E.P., Steel, R.J., 2009. Shelf edge and shoreline trajectories, a dynamic approach to stratigraphic analysis. Basin Research 21, 445–453.
Henriksen, S., Helland-Hansen, W., Bullimore, S., 2011a. Relationships between shelf-edge trajectories and sediment dispersal along depositional dip and strike: a different approach to sequence stratigraphy. Basin Research 23, 3–21.
Henriksen, S., Pontén, A., Janbu, N., Paasch, B., 2011b. The importance of sediment supply and sequence-stacking pattern in creating hyperpycnal flows. In: Slatt, R.M., Zavala, C. (Eds.), Sediment Transfer from Shelf to Deep Water—Revisiting the Delivery System. American Association of Petroleum Geologists Studies in Geology, pp. 129–152.
Houseknecht, D.W., Bird, K.J., Schenk, C.J., 2009. Seismic analysis of clinoform depositional sequences and shelf-margin trajectories in Lower Cretaceous (Albian) strata, Alaska North Slope. Basin Research 21, 644–654.
Hui, F., Xu, B., Huang, H., Yu, Q., Gong, P., 2008. Modelling spatial–temporal change of Poyang Lake using multitemporal Landsat imagery. International Journal of Remote Sensing 29, 5767–5784.
Huybers, K., Rupper, S., Roe, G.H., 2016. Response of closed basin lakes to interannual climate variability. Climate Dynamics 46, 3709–3723.
Ji, Y., Ren, H., Zhang, S., Ma, Z., Niu, J., Guo, S., Gao, C., Liu, X., 2022. Paleogene palaeogeography and oil and gas distribution in Bohai Bay Basin. Journal of Palaeogeography (Chinese Edition) 24, 611–633 (in Chinese with English Abstract).
Johannessen, E.P., Steel, R.J., 2005. Shelf-margin clinoforms and prediction of deepwater sands. Basin Research 17, 521–550.
Johnson, T.C., Halfman, J.D., Rosendahl, B.R., Lister, G.S., 1987. Climatic and tectonic effects on sedimentation in a rift-valley lake: evidence from high-resolution seismic profiles, Lake Turkana, Kenya. Geological Society of America Bulletin 98, 439–447.
Kroonenberg, S.B., Rusakov, G.V., Svitoch, A.A., 1997. The wandering of the Volga delta: a response to rapid Caspian sea-level change. Sedimentary Geology 107, 189–209.
Lamb, M.P., McElroy, B., Kopriva, B., Shaw, J., Mohrig, D., 2010. Linking river-flood dynamics to hyperpycnal-plume deposits: experiments, theory, and geological implications. Geological Society of America Bulletin 122, 1389–1400.
Li, S., Zhu, H., Xu, C., Zeng, H., Liu, Q., Yang, X., 2019. Seismic-based identification and stage analysis of overlapped compound sedimentary units in rifted lacustrine basins: an example from the Bozhong sag, Bohai Bay Basin, China. American Association of Petroleum Geologists Bulletin 103, 2521–2543.
Li, S., Zhu, H., Yang, X., Xu, C., 2021. Seismic geomorphology, architecture and genesis of unusual confined and semiconfined sedimentary units on the northern slope of the Bonan uplift, Bohai Bay Basin, China. Journal of Petroleum Science and Engineering 196, 107696. https://doi.org/10.1016/j.petrol.2020.107696.
Lin, C., Jiang, J., Shi, H., Zhang, Z., Liu, J., Qin, C., Li, H., Ran, H., Wei, A., Tian, H., Xing, Z., Yao, Q., 2018. Sequence architecture and depositional evolution of the northern continental slope of the South China Sea: responses to tectonic processes and changes in sea level. Basin Research 30 (Suppl. 1), S568–S595.
Liu, E., Wang, H., Li, Y., Zhou, W., Leonard, N.D., Lin, Z., Ma, Q., 2014. Sedimentary characteristics and tectonic setting of sublacustrine fans in a half-graben rift depression, Beibuwan Basin, South China Sea. Marine and Petroleum Geology 53, 9–21.
Liu, E., Wang, H., Feng, Y., Pan, S., Jing, Z., Ma., Q., Gan, H., Zhao, J., 2020a. Sedimentary architecture and provenance analysis of a sublacustrine fan system in a half-graben rift depression of the South China Sea. Sedimentary Geology 409, 105781. https://doi.org/10.1016/j.sedgeo.2020.105781.
Liu, J., Xian, B., Ji, Y., Gong, C., Wang, J., Wang, Z., Chen, P., Song, D., Wei, W., Zhang, X., Dou, L., 2020b. Alternating of aggradation and progradation dominated clinothems and its implications for sediment delivery to deep lake: the Eocene Dongying Depression, Bohai Bay Basin, east China. Marine and Petroleum Geology 114, 104197. https://doi.org/10.1016/j.marpetgeo.2019.104197.
Lyons, R.P., Scholz, C.A., Buoniconti, M.R., Martin, M.R., 2011. Late Quaternary stratigraphic analysis of the Lake Malawi Rift, East Africa: an integration of drill-core and seismic-reflection data. Palaeogeography, Palaeoclimatology, Palaeoecology 303, 20–37.
Meng, Q., Liu, Z., Bruch, A.A., Liu, R., Hu, F., 2012. Palaeoclimatic evolution during Eocene and its influence on oil shale mineralisation, Fushun Basin, China. Journal of Asian Earth Sciences 45, 95–105.
Mitchum, R.M., Wagoner, J.C.V., 1991. High-frequency sequences and their stacking patterns: sequence-stratigraphic evidence of high-frequency eustatic cycles. Sedimentary Geology 70, 131–160.
Moradi, A.V., Sarı, A., Akkaya, P., 2016. Geochemistry of the Miocene oil shale (Hançili Formation) in the Çankırı–Çorum Basin, Central Turkey: implications for paleoclimate conditions, source-area weathering, provenance and tectonic setting. Sedimentary Geology 341, 289–303.
Neal, J.E., Abreu, V., 2009. Sequence stratigraphy hierarchy and the accommodation succession method. Geology 37, 779–782.
Neal, J.E., Abreu, V., Bohacs, K.M., Feldman, H.R., Pederson, K.H., 2016. Accommodation succession (δA/δS) sequence stratigraphy: observational method, utility and insights into sequence boundary formation. In: Bruce, H., Norman, C.R., Dorene, W., Anthony, D., Carlo, M., Michael, H., Richard, W. (Eds.), Sequence Stratigraphy: Future Defined. Journal of the Geological Societyvol. 173, pp. 803–816.
Olariu, C., Zhang, Z., Zhou, C., Yuan, X., Steel, R.J., Chen, S., Zhang, J., Chen, D., 2022. Conglomerate to mudstone lacustrine cycles revealed in Junggar Basin, Northwest China: Middle Permian Lucaogou and Jingjingzigou formations. Marine and Petroleum Geology 136, 105473. https://doi.org/10.1016/j.marpetgeo.2021.105473.
Paumard, V., Bourget, J., Payenberg, T., Ainsworth, R.B., George, A.D., Lang, S., Posamentier, H.W., Peyrot, D., 2018. Controls on shelf-margin architecture and sediment partitioning during a syn-rift to post-rift transition: insights from the Barrow Group (Northern Carnarvon Basin, North West Shelf, Australia). Earth-Science Reviews 177, 643–677.
Paumard, V., Bourget, J., Payenberg, T., George, A.D., Ainsworth, R.B., Lang, S., 2019. From quantitative 3D seismic stratigraphy to sequence stratigraphy: insights into the vertical and lateral variability of shelf-margin depositional systems at different stratigraphic orders. Marine and Petroleum Geology 110, 797–831.
Pellegrini, C., Patruno, S., Helland-Hansen, W., Steel, R.J., Trincardi, F., 2020. Clinoforms and clinothems: fundamental elements of basin infill. Basin Research 32, 187–205.
Qi, K., Gong, C., Zhang, J., Andresen, K.J., Jin, Z., 2023. Relative sea-level control on the building of two distinct shelf-margin clinothems on the late-Quaternary Pearl River margin: insights from numerical stratigraphic forward modelling. Basin Research 35, 842–864.
Qin, Y., Zhu, X., Zhu, S., Mcelroy, B., 2021. Impact of deep-time palaeoclimate on the sedimentary records and morphology of lacustrine shoal-water deltas, Upper Eocene Dongying Depression, Bohai Bay Basin, China. Sedimentology 68, 3253–3278.
Shankman, D., Keim, B.D., Song, J., 2006. Flood frequency in China's Poyang Lake region: trends and teleconnections. International Journal of Climatology 26, 1255–1266.
Sømme, T.O., Jackson, C.A.L., 2013. Source-to-sink analysis of ancient sedimentary systems using a subsurface case study from the Møre–Trøndelag area of southern Norway: part 2—sediment dispersal and forcing mechanisms. Basin Research 25, 512–531.
Sømme, T.O., Helland-Hansen, W., Martinsen, O.J., Thurmond, J.B., 2009. Relationships between morphological and sedimentological parameters in source-to-sink systems: a basis for predicting semiquantitative characteristics in subsurface systems. Basin Research 21, 361–387.
Sztanó, O., Szafián, P., Magyar, I., Horányi, A., Bada, G., Hughes, D.W., Hoyer, D.L., Wallis, R.J., 2013. Aggradation and progradation controlled clinothems and deep-water sand delivery model in the Neogene Lake Pannon, Makó Trough, Pannonian Basin, SE Hungary. Global and Planetary Change 103, 149–167.
Tao, S., Xu, Y., Tang, D., Xu, H., Li, S., Chen, S., Liu, W., Cui, Y., Gou, M., 2017. Geochemistry of the Shitoumei oil shale in the Santanghu Basin, Northwest China: implications for paleoclimate conditions, weathering, provenance and tectonic setting. International Journal of Coal Geology 184, 42–56.
Wang, R., Shi, W., Xie, X., Wang, L., Manger, W., Busbey, A.B., Xu, Q., 2017. Lower Cretaceous lacustrine succession, North Yellow Sea Basin, eastern China: rift basin sequence stratigraphy and stacking patterns in response to magmatic activity. Marine and Petroleum Geology 88, 531–550.
Wignall, P.B., Twitchett, R.J., 1996. Oceanic anoxia and the End Permian mass extinction. Science 272, 1155–1158.
Wu, Q., Xian, B., Gao, X., Bai, Q., Wang, Z., Liu, J., Chen, P., Li, Y., Rahman, N.U., Tian, R., Zhang, W., Zhang, H., 2022. Differences of sedimentary triggers and depositional architecture of lacustrine turbidites from normal regression to forced regression: Eocene Dongying depression, Bohai Bay Basin, East China. Sedimentary Geology 439, 106222. https://doi.org/10.1016/j.sedgeo.2022.106222.
Wu, Q., Xian, B., Gao, X., Tian, R., Zhang, H., Liu, J., Gao, Y., Wang, P., 2023. Diversity of depositional architecture and sandbody distribution of sublacustrine fans during forced regression: a case study of Paleogene Middle Sha 3 Member in Dongying Sag, Bohai Bay Basin, East China. Petroleum Exploration and Development 50, 894–908.
Würtzen, C.L., Osmond, J.L., Faleide, J.I., Nystuen, J.P., Anell, I.M., Midtkandal, I., 2022. Syn- to post-rift alluvial basin fill: seismic stratigraphic analysis of Permian–Triassic deposition in the Horda Platform, Norway. Basin Research 34, 883–912.
Xia, S., Lin, C., Wu, W., Du, X., 2022. Sequence architecture, depositional evolution and responses to tectonic subsidence and lacustrine fluctuation in lacustrine rift basin: a case study from Cenozoic Liaodong Bay, Bohai Bay Basin. Journal of Petroleum Science and Engineering 208, 109494. https://doi.org/10.1016/j.petrol.2021.109494.
Xu, C., Huan, L., Song, Z., Jia, D., 2020. Sequence stratigraphy of the lacustrine rift basin in the Paleogene system of the Bohai Sea area: architecture mode, deposition filling pattern, and response to tectonic rifting processes. Interpretation 8, 2324–8858.
Yang, W., Zhu, D., Yin, Y., Ding, J., 2015. Geochemical restoration of paleo-water depth and its application to sequence stratigraphy. Geological Review 61 (Suppl. 1), S756–S757 (in Chinese with English Abstract).
Yang, H., Liu, C., Wang, F., Tang, G., Li, G., Zeng, X., Wu, Y., 2021. Paleoenvironment and development model of source rocks of Dongying Formation in Bozhong Sag. Lithologic Reservoirs 33, 81–92 (in Chinese with English Abstract).
Yang, T., Cao, Y., Wang, Y., Cai, L., Liu, H., Jin, J., 2023a. Sedimentary characteristics and depositional model of hyperpycnites in the gentle slope of a lacustrine rift basin: a case study from the third member of the Eocene Shahejie Formation, Bonan Sag, Bohai Bay Basin, Eastern China. Basin Research 35, 1590–1618.

Yang, T., Cao, Y., Liu, H., 2023b. Highstand sublacustrine fans: the role of a sudden increase in sediment supply. Basin Research 35, 1486–1508.
Yu, Y., Zhou, X., Xu, C., Wu, K., Lv, D., Liu, Y., Zhou, X., 2020. Architecture and evolution of the Cenozoic offshore Bohai Bay basin, eastern China. Journal of Asian Earth Sciences 192, 104272. https://doi.org/10.1016/j.jseaes.2020.104272.
Yu, Y., Gong, C., Li, D., Liu, P., Li, Y., 2021. The pivotal but underappreciated role of time scales on clinothem-based prediction of sediment dispersal to deepwater: insights derived from greenhouse clinothem pairs in the Bohai Bay Basin. Marine and Petroleum Geology 127, 104967. https://doi.org/10.1016/j.marpetgeo.2021.104967.
Zavala, C., Arcuri, M., 2016. Intrabasinal and extrabasinal turbidites: origin and distinctive characteristics. Sedimentary Geology 337, 36–54.
Zavala, C., Ponce, J.J., Arcuri, M., Drittanti, D., Freije, H., Asensio, M., 2006. Ancient lacustrine hyperpycnites: a depositional model from a case study in the Rayoso Formation (Cretaceous) of west-central Argentina. Journal of Sedimentary Research 76, 41–59.
Zhang, J., Kim, W., Olariu, C., Steel, R.J., 2019. Accommodation- versus supply-dominated systems for sediment partitioning to deep water. Geology 47, 419–422.
Zhang, J., Olariu, C., Steel, R.J., Kim, W., 2020. Climatically controlled lacustrine clinoforms: theory and modelling results. Basin Research 32, 240–250.
Zhao, X., Gong, C., Zhou, L., Li, D., Pu, X., Han, G., Jin, F., Yu, Y., Jiang, W., Dong, X., 2021. Topset-to-foreset rollover trajectories as reliable predictors of sediment-volume partitioning into deep-lake areas. Petroleum Science 18, 712–727.
Zhu, H., Yang, X., Zhou, X., Liu, K., 2014. Three-dimensional facies architecture analysis using sequence stratigraphy and seismic sedimentology: example from the Paleogene Dongying Formation in the BZ3-1 block of the Bozhong Sag, Bohai Bay Basin, China. Marine and Petroleum Geology 51, 20–33.
Zhu, Y., Liu, S., Zhang, B., Gurnis, M., Ma, P., 2021. Reconstruction of the Cenozoic deformation of the Bohai Bay Basin, North China. Basin Research 33, 364–381.